NARSIS

New Approach to Reactor Safety ImprovementS

WP4: Applying and comparing various safety assessment approaches on a virtual reactor

Del4.2 - Metamodels for seismic and tsunami risk analyses

This project has received funding from the Euratom research and training programme 2014-2018 under Grant Agreement No. 755439.

Project Acronym:	NARSIS
Project Title:	New Approach to Reactor Safety Improvements
Deliverable:	Del4.2 - Metamodels for seismic and tsunami risk analyses
Month due:	32
Month delivered:	33
Leading Partner:	Électricité de France (EDF)
Version:	V4

Primary Authors: Cyril Feau (CEA), Jeremy Rohmer (BRGM), Zhiyi Wang (EDF)
Irmela Zentner (EDF)
Others contributors:

Deliverable Review:
Reviewer: Giuseppe Rastiello (CEA)
Date:

Dissemination Level		
PU	Public	X
PP	Restricted to other programme participants (including the Commission Services)	
RE	Restricted to a group specified by the consortium (including the Commission Services)	
CO	Confidential, only for members of the consortium (including the Commission Services)	

Table of contents

List of Figures

List of Tables

Acronyms

ALS Associated Linear System.

ANN Artificial Neural Networks.

ASA Average Spectral Acceleration.

BEM Boundary Element Method.

CAV Cumulative Absolute Velocity.

CI Confidence Interval.

DMs Damage Measures.

ELM Equivalent Linear Method.

FEM Finite Element Method.

HDMR High-Dimensional Model Representation.

IM Intensity Measure.

IRF Impulse Response Function.

K-K Kashiwazaki-Kariwa.

KDE Kernel Density Estimation.

LHS Latin Hypercube Sampling.

MC Monte Carlo.

MPI Message Passing Interface.

NCOE Niigataken-Chuetsu-Oki earthquake.

NPP Nuclear Power Plant.

PGA Peak Ground Acceleration.

PGD Peak Ground Displacement.

PGV Peak Ground Velocity.

PI Prediction Interval.

RMSE Root-Mean-Square Error.

RV Random Variables.

SSE Sea Surface Elevation.

SSI Soil-Structure Interaction.

SVM Support Vector Machines.

1 Introduction

Metamodels allow reducing computational costs when the best-estimate natural hazard analyses require heavy numerical calculations to compute the level of threat and structural response in a probabilistic framework. For example, the computation seismic fragility curves requires a large number of structural response analyses (ranging from hundreds to several millions depending on the methodology applied) to evaluate the failure probabilities.However, a large number of structural analyses is not feasible when considering complex models for structures and equipment, as it is the case in nuclear safety analyses.

The construction of a metamodel consists of developing for a simplified expression between model input and output to allow for probabilistic and sensitivity analyses at an affordable computational cost. The input parameters are the so-called intensity measures (IMs). The latter are proxies such as peak ground acceleration or the energy of the signal, and they express the nocivity of the earthquake. In consequence, a first step in the metamodelling procedure consists in selecting the most pertinent proxy(ies) to represent the seismic load. Due to the reduction of the complex ground motion time histories to a scalar/vector IM, it is clear that even for a given set of input parameters, there is remaining variability in the model output (e.g., two-time histories with the same PGA might lead to different structural responses). This is called the prediction uncertainty; depending on the adequateness of the IMs, it can be more or less important and has to be accounted for in the metamodelling approach.

The model output can be continuous quantities such as an admissible strain level, spectral acceleration at floor level, or discrete failure indicators (e.g., buckling, etc). In nuclear practice, a lognormal distribution is generally adopted to develop fragility curves. This modeling choice can be assessed and possibly confirmed thanks to the metamodel. In what follows, we provide two new approaches for metamodelling strategies for seismic fragility analyses to tackle the different aspects of metamodelling for fragility analyses.

On the other hand, although tsunami hazard assessments are typically based on worst-case scenarios (e.g., [2]), these scenarios are based on a large variety of information sources, they remain uncertain. To account for these uncertainties, a key pillar is to conduct different simulations by testing different parameters' configurations. Yet, the difficulty is related to the computation time cost of the numerical simulator, which can be very high (typically several hours). In this situation, metamodels can be a good option to overcome this computational burden (e.g., [3]).

2 Metamodels for seismic fragility analyses

Fragility curves are computed as conditional probabilities of failure of structures, or critical components, for given values of a seismic IM (e.g., the Peak Ground Acceleration, PGA) [4]). The computation of fragility curves requires a realistic estimation of the structure performance subject to seismic excitations via the quantification and the propagation of uncertainties existing in earthquake ground motions, structural material properties, etc.

These uncertainties are categorized into two groups [5]:

- aleatory uncertainties, which reveal the inherent randomness of variables or stochastic processes,
- and epistemic uncertainties, which originate from the lack of knowledge about the model and provide a family of confidence interval curves for the fragility estimation.

The distinction of the aleatory and epistemic uncertainties allows for determining confidence intervals for fragility curves and has a major impact on the High Confidence Low Probability of Failure (HCLPF) capacity of the analysed equipment.

This conditional probability can be evaluated pointwise for different IM values using the Monte Carlo method [6, 7], as well as with methods based on the log-normal hypothesis [5, 8, 9]. However, both methods require a few hundred heavy numerical simulations with the Finite Element Method (FEM).

One way reduce such computational costs consists in building a metamodel to calibrate the statistical relation between seismic inputs and structural outputs. Some studies regarding the application of metamodels in fragility analysis have been realized recently. Most of them focus on using seismic IMs to characterize earthquake accelerations.

Metamodels are constructed to calibrate the relation between Damage Measures (DMs) and uncertain inputs of the structural models, including IMs and material parameters. The construction of the metamodels is either achieved by decomposing the nonlinear input-output relation with High-Dimensional Model Representation (HDMR) [10, 11], or realized with polynomial regression [12, 13, 14, 15, 16]. Alternatively one can use more advanced statistical tools, such as Artificial Neural Networks (ANN) [17, 18, 19, 20, 21], LASSO regression [22], Bayesian networks [23], merging multivariate adaptive regression splines, radial basis function network, support vector regression [24], Kriging [25, 26], etc.

On the other hand, earthquake accelerations are also used directly as inputs of the metamodel [27] to predict structural response time histories. The construction of the metamodel is divided into two steps: the first step is to extract the characteristics of earthquake motions with nonlinear auto-regression; then, the polynomial chaos expansion is applied to these characteristics to construct the metamodel. DMs are computed from the structural response time histories, and fragility curves can thus be obtained. Although this method seems different from the classical metamodeling with IMs, the idea remains the same: the nonlinear auto-regression serves as a tool to extract the features of earthquake motions and past values of the structural displacement, while these features are represented by the IMs in classical approaches. Besides regression methods, classification models like logistic regression, random forests, and support vector machine are utilized in [28] to predict the probability of failure from the uncertain inputs directly.

In what follows, we present two approaches to speed up the computation of fragility curves by numerical simulation by making use of metamodels.

2.1 SVM-based methodology

Recently, Sainct et al. [1] have proposed a methodology based on Support Vector Machines (SVMs) coupled with an Active Learning algorithm to estimate efficiently seismic fragility curves. In practice, the input excitation is reduced to some relevant IMs, and then SVMs are used for binary classification of the structural responses relative to a limit threshold of exceedance. Since the output is not binary but a real-valued score, a probabilistic interpretation of the output is exploited to estimate fragility curves as score functions. Thus, with appropriate kernels, the score function can be viewed as an efficient IM (see, e.g., [29]) since a perfect classifier would lead to a fragility curve in the form of a unit step function when the problem is linearly separable. This methodology also allows deriving fragility curves easily as functions of classical IMs (e.g., PGA).

2.1.1 Model of earthquake ground motion

In order to illustrate the methodology, the seismic ground motion model defined in [30] was implemented. In this model, a seismic ground motion $s(t)$ with $t \in [0, T]$ is modeled as:

$$s(t) = q(t, \boldsymbol{\alpha}) \left[\frac{1}{\sigma_f(t)} \int_{-\infty}^{t} h[t - \tau, \boldsymbol{\beta}(\tau)] w(\tau) d\tau \right], \tag{1}$$

where $q(t, \boldsymbol{\alpha})$ is a deterministic, non-negative modulating function that is defined as:

$$q(t, \boldsymbol{\alpha}) = \begin{cases} \alpha_1 t^2 / T_1^2 & \text{if} \quad 0 \leq t \leq T_1, \\ \alpha_1 & \text{if} \quad T_1 \leq t \leq T_2, \\ \alpha_1 \exp\left[-\alpha_2 (t - T_2)^{\alpha_3}\right] & \text{if} \quad T \geq t \geq T_2, \end{cases} \tag{2}$$

and that depends on the vector-valued parameter $\boldsymbol{\alpha} = (\alpha_1, \alpha_2, \alpha_3, T_1, T_2) \in \mathbb{R}_+^5$. In Eq. (1), terms inside the squared brackets represent a filtered white-noise process of unit variance.Function, $w(t)$ is a white-noise process and $h(t, \boldsymbol{\beta})$ is the Impulse Response Function (IRF) of the linear filter that depends on the vector-valued parameter $\boldsymbol{\beta}$. Moreover,

$$\sigma_f^2(t) = \int_{-\infty}^{t} h^2(t - \tau, \boldsymbol{\beta}(\tau)) d\tau \tag{3}$$

is the variance of the process defined by the integral in Eq. (1). Finally, in order to achieve spectral nonstationarity of the ground motion, the parameter $\boldsymbol{\beta}$ is allowed to depend on the time τ.

Following [30], the IRF is of the form:

$$h[t - \tau, \boldsymbol{\beta}(\tau)] = \frac{\omega_f(\tau)}{\sqrt{1 - \zeta_f^2}} \exp\left[-\zeta_f \omega_f(\tau)(t - \tau)\right] \sin\left[\omega_f(\tau) \sqrt{1 - \zeta_f^2}(t - \tau)\right] \mathbf{1}_{t \geq \tau}, \tag{4}$$

where $\boldsymbol{\beta}(\tau) = [\omega_f(\tau), \zeta_f]$, $\omega_f(\tau)$ is the natural frequency (that depends on the time τ), $\zeta_f \in [0, 1]$ is the (constant) damping ratio and $\mathbf{1}_{t \geq \tau}$ is the indicator function such that $\mathbf{1}_{t \geq \tau}$ is equal to unity if $t \geq \tau$ and is equal to zero otherwise. A linear form is chosen for the frequency:

$$\omega_f(\tau) = \omega_0 + \frac{\tau}{T}(\omega_n - \omega_0). \tag{5}$$

The IRF is, therefore, parameterized by $\boldsymbol{\lambda} = (\omega_0, \omega_n, \zeta_f) \in \mathbb{R}_+^3$.

The modulation parameters $\boldsymbol{\alpha}$ and the filter parameters $\boldsymbol{\lambda}$ are identified independently following the procedure proposed in [31, 30] for the $N_\mathrm{r} = 97$ acceleration records selected from the European Strong Motion Database [32] in the domain $5.5 < M < 6.5$ and $R < 20\mathrm{km}$ (M being the magnitude and R the distance from the epicenter).

The identification of the model parameters $\boldsymbol{\theta} = (\boldsymbol{\alpha}, \boldsymbol{\lambda})$ for each of the $N_\mathrm{r} = 97$ acceleration records, gives N_r data points $(\boldsymbol{\theta_i})_{i=1}^{N_\mathrm{r}}$ in the parameter space $\mathbb{R}_+^8$. The model then allows to generate artificial signals, thanks to the white-noise. In order to estimate fragility curves, a second level of randomness is added in the generation process, coming from the parameters $\boldsymbol{\theta}$ themselves. So, the parameters' probability distribution function is estimated using a Gaussian Kernel Density Estimation (KDE) method [33]:

$$p_{KDE}(\boldsymbol{\theta}) = \frac{1}{N_\mathrm{r}} \sum_{i=1}^{N_\mathrm{r}} \phi_{\mathbf{H}}(\boldsymbol{\theta} - \boldsymbol{\theta_i}), \tag{6}$$

where $\phi_{\mathbf{H}}$ is a Gaussian kernel centered at 0 with covariance matrix $\mathbf{H}$ properly chosen from the data points $(\boldsymbol{\theta_i})_{i=1}^{N_\mathrm{r}}$ (see [33]). In this work $N_\mathrm{s} = 10^5$ artificial seismic ground motions $s_i(t)$ are generated.

2.1.2 Model of the mechanical structure

For the illustrative application of the methodology, a nonlinear single degree of freedom system was considered. Indeed, despite its extreme simplicity, such model may reflect the essential features of the nonlinear responses of some real structures. Moreover, in a probabilistic context requiring Monte Carlo

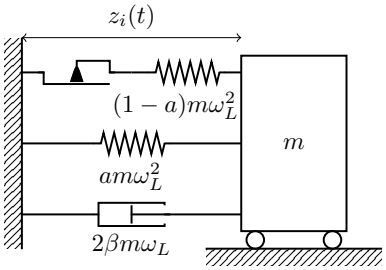

Figure 1: Rheological hysteretic model of the nonlinear oscillator

simulations, it makes it possible to have reference results with reasonable numerical cost. Its equation of motion reads:

$$\ddot{z}_i(t) + 2\beta\omega_L \dot{z}_i(t) + f_i^{nl}(t) = -s_i(t), \quad i \in [\![1, N_s]\!] \tag{7}$$

where $\dot{z}_i(t)$ and $\ddot{z}_i(t)$ are respectively the relative velocity and acceleration of the unit mass of the system submitted to the i-th artificial seismic ground motion $s_i(t)$ with null initial conditions in velocity and displacement. In equation 7, β is the damping ratio, $\omega_L = 2\pi f_L$ is the circular frequency and $f_i^{nl}(t)$ is the nonlinear resisting force.

The rheological hysteretic model of the oscillator, defining kinematic hardening, is presented in Figure 1. In this study, $f_L = 5$ Hz, $\beta = 2\%$, the yield limit is $Y = 5.10^{-3}$ m, and the post-yield stiffness $am\omega_L^2$ is equal to 20% of the elastic stiffness ($m\omega_L^2$), that is $a = 0.2$.

Moreover, we call $\tilde{z}_i(t)$ the relative displacement of the Associated Linear System (ALS, $a = 1$ see Figure 1), that is assumed to be known. Its equation of motion is:

$$\ddot{\tilde{z}}_i(t) + 2\beta\omega_L \dot{\tilde{z}}_i(t) + \omega_L^2 \tilde{z}_i(t) = -s_i(t), \tag{8}$$

Finally, we set:

$$Z_i = \max_{t\in[0,T]} |z_i(t)|, \tag{9}$$

and

$$L_i = \max_{t\in[0,T]} |\tilde{z}_i(t)|. \tag{10}$$

2.1.3 Choice of the seismic IM indicators

A complete review of the existing seismic IM indicators can be found in [29]. The methodology presented here is intended to take into account the advantage of using a ground motion parametric model, in considering its constitutive parameters as input parameters of a metamodel. Thus, if $\mathcal{B} = (s_i(t))_{i\in[\![1,N_s]\!]}$ is the database of N_s simulated ground motions, we can consider $\boldsymbol{\theta_i} = (\boldsymbol{\alpha}_i, \boldsymbol{\lambda}_i) \in \mathbb{R}_+^8$ the associated modulating and filter parameters as inputs. However, they can not be used alone since there is an infinity of possible realizations of the stochastic process for a set of parameters, due to the white-noise process. They have to be used additionally with the main classical IM parameters. Thus, for every signal $s_i(t)$, we also consider:

1. the Peak Ground Acceleration : $PGA_i = \max_{t\in[0,T]} |s_i(t)|$;
2. the Peak Ground Velocity : $V_i = \max_{t\in[0,T]} \left|\int_0^t s_i(\tau)d\tau\right|$;
3. the Peak Ground Displacement : $D_i = \max_{t\in[0,T]} \left|\int_0^t \int_0^\tau s_i(u)du d\tau\right|$;
4. the total energy $E_i = \int_0^T s_i^2(\tau)d\tau$ (this IM parameter is proportional to the "Arias Intensity" indicator usually considered);
5. the linear displacement L_i. The PSA, $\omega_L^2 L_i$ is usually considered as IM indicator, nevertheless, since the variable of interest is a nonlinear displacement, it is more suitable to use linear displacement.

So, each signal $s_i(t)$ is represented by a vector $\boldsymbol{X}_i^\star = (\boldsymbol{\alpha}_i, \boldsymbol{\lambda}_i, PGA_i, V_i, D_i, E_i, L_i) \in \mathbb{R}_+^{13}$ in order to predict whether the nonlinear displacement Z_i is greater than a damage state threshold (e.g., twice the yield displacement Y).

2.1.4 Preprocessing of the training data

First of all, recall that $N_{\mathrm{s}} = 10^5$ signals have been generated and, for each of them, the displacement L_i of the ALS have been calculated.

Signals with very small or very large values of L are discarded from the database. Indeed, on the one hand, the signals which produce values of L lower than the yield displacement Y are not useful, because the structural responses do not reach the limit threshold $2Y$: if $L_i < Y$, then $Z_i = L_i < Y$. This discards 66% of the N_{s} signals. On the other hand, the very few signals which produce very large values of L ($L_i > 6Y$) are also discarded because the mechanical model is not realistic beyond that level.

This gives a subset I of the database, composed of $N = 33718$ signals, such that $\forall i \in I$, $L_i \in [Y, 6Y]$.

In addition, a Box-Cox transform is applied to each of the thirteen entries of $\boldsymbol{X}_i^\star = (\boldsymbol{\alpha}_i, \boldsymbol{\lambda}_i, PGA_i, V_i, D_i, E_i, L_i) \in \mathbb{R}_+^{13}$. This nonlinear step is critical for the accuracy of the classification, especially for linear SVM classifiers. The Box-Cox transform (parameterized by $\delta \in [0, +\infty)$) reads:

$$\mathrm{BC}_\delta(x) = \begin{cases} \dfrac{x^\delta - 1}{\delta} & \text{if } \delta \neq 0, \\ \log(x) & \text{if } \delta = 0. \end{cases} \tag{11}$$

The parameter δ is optimized, for each entry, in order to obtain an empirical distribution as close as possible to the normal law by maximizing the log-likelihood. Finally, all of the thirteen components are standardized, thus forming the training database $\boldsymbol{\mathcal{X}} = \{\boldsymbol{X_1}, \ldots, \boldsymbol{X_N}\}$ with $\boldsymbol{X_i} \in \mathbb{R}^{13}$.

2.1.5 Support Vector Machines

In machine learning, SVMs are supervised learning models used for classification and regression analysis. In the linear binary classification setting, given a training data set $\{\boldsymbol{X_1}, \ldots, \boldsymbol{X_n}\}$ that are vectors in $\mathbb{R}^d$, and their labels $\{l_1, \ldots, l_n\}$ in $\{-1, 1\}$, the SVM is a hyperplane of $\mathbb{R}^d$ that separates the data by a maximal margin.

More generally, SVMs allow one to project the original training data set $\{\boldsymbol{X_1}, \ldots, \boldsymbol{X_n}\}$ onto a higher dimensional feature space via a Mercer kernel operator K. The classifier then associates to each new signal $\boldsymbol{X}$ a score $f_n(\boldsymbol{X})$ given by $f_n(\boldsymbol{X}) = \sum_{i=1}^n \varphi_i K(\boldsymbol{X_i}, \boldsymbol{X})$. A new seismic signal, represented by the vector $\boldsymbol{X}$, has an estimated label $\hat{l}$ of 1 if $f_n(\boldsymbol{X}) > 0$, -1 otherwise.

In a general SVM setting, most of the labeled instances $\boldsymbol{X_i}$ have an associated coefficient φ_i equal to 0; the few vectors $\boldsymbol{X_i}$ such that $\varphi_i \neq 0$ are called "support vectors", hence the name "support vector machine". This historical distinction among labeled instances is less relevant in the case of active learning, since most of the φ_i are non-zero. In the linear case, $K(\boldsymbol{X_i}, \boldsymbol{X})$ is the scalar product in $\mathbb{R}^d$, and the score is:

$$f_n(\boldsymbol{X}) = \boldsymbol{W}^\top \boldsymbol{X} + c, \tag{12}$$

where $\boldsymbol{W} \in \mathbb{R}^d$ and $c \in \mathbb{R}$ depend on the coefficients φ_i.

2.1.6 Active learning

In the case of pool-based active learning, in addition to the labeled set $\boldsymbol{\mathcal{L}} = \{\boldsymbol{X_1}, \ldots, \boldsymbol{X_n}\}$, we have,access to a set of unlabeled samples $\boldsymbol{\mathcal{U}} = \{\boldsymbol{X_{n+1}}, \ldots, \boldsymbol{X_N}\}$ (therefore $\boldsymbol{\mathcal{X}} = \boldsymbol{\mathcal{L}} \cup \boldsymbol{\mathcal{U}}$). We assume that there exists a way to provide a label for any sample $\boldsymbol{X_i}$ from this set (in our case, running a full simulation of the physical model using signal $s_i(t)$), but the labeling cost is high. After labeling a sample, we simply add it to the training set.

In order to improve a classifier it seems intuitive to query labels for samples that cannot be easily classified. Various querying methods are possible [34, 35]. The method presented here only requires to compute the score $f_n(\boldsymbol{X})$ for the samples in the unlabeled set, then to identify a sample that reaches the minimum of the absolute value $|f_n(\boldsymbol{X})|$, since a score close to 0 means a high uncertainty for this sample.

The algorithm starts with $n = 2$ samples with indices j_1 and j_2, labeled $+1$ and -1. Recursively, if the labels of signals $j_1, \ldots, j_n$ are known, it consists in:

1. computing the SVM classifier associated with the labeled set $\{(\boldsymbol{X_{j_1}}, l_{j_1}), \ldots, (\boldsymbol{X_{j_n}}, l_{j_n})\}$;
2. computing the score $f_n(\boldsymbol{X_i})$ for each unlabeled instance $\boldsymbol{X_i}$, $i \in [\![1, N]\!] \backslash \{j_1, \ldots, j_n\}$;
3. identifying the instance with maximum uncertainty for this classifier:

$$j_{n+1} = \underset{i \in [\![1,N]\!] \backslash \{j_1,\ldots,j_n\}}{\operatorname{argmin}} |f_n(\boldsymbol{X_i})|, \tag{13}$$

   and computing the corresponding displacement $Z_{j_{n+1}}$ by running a full simulation of the mechanical model;
4. adding the instance $(\boldsymbol{X_{j_{n+1}}}, l_{j_{n+1}} = \operatorname{sgn}(Z_{j_{n+1}} - 2Y))$ to the labeled set.

No termination criteria are explicitly given here because, in practice, the limitation regarding the number of training data available is mainly due to the computational cost of the numerical mechanical calculations.

2.1.7 Fragility Curves estimations

Different procedures can be used to construct non-parametric fragility curves [8, 6, 36]. Here, they are constructed based on k-means clustering of the IM data [36].

In a Monte Carlo-based approach this means that in each cluster, the empirical probability of failure is evaluated by the ratio between the number of structural responses that exceed the limit threshold and the number of structural responses belonging to the cluster.

With SVM classifiers which give to each signal $s_i(t)$ a real-valued score $f_n(\boldsymbol{X_i})$ whose sign expresses the estimated label, we first need to assign a probability to estimate fragility curves. For a perfect classifier, the probability would be 0 if $f_n(\boldsymbol{X}) < 0$ and 1 if $f_n(\boldsymbol{X}) > 0$. In that case, a logistic function is used in order to get a probablity in $(0, 1)$:

$$p_n(\boldsymbol{X}) = \frac{1}{1 + \exp[-a f_n(\boldsymbol{X}) + b]}, \tag{14}$$

where a and b are the slope and intercept parameters of the logistic function (b should be close to 0 if the classifier has no bias, giving a probability of $1/2$ to signals with $f_n(\boldsymbol{X}) \approx 0$). These parameters are estimated by maximizing the likelihood function from Eq. (14) on the labeled set $\{(\boldsymbol{X_{j_1}}, l_{j_1}), \ldots, (\boldsymbol{X_{j_n}}, l_{j_n})\}$.

The estimation of the score-based fragility curve is given by Eq. (14). If we are interested in more-understandable fragility curves such as PGA-based fragility curves (or an other IM-based fragility curves), the classifier should first be used to predict the scores and the associated probabilities by Eq. (14) of several new input parameters. These new input parameters correspond to those which were not selected for the construction of the classifier, or other ones generated from new simulations of the seismic ground motion model. If we consider this probability as a function of four parameters ($p_n(L, V, PGA, \omega_0)$ if $\boldsymbol{X} \in \mathbb{R}^4$), then any of those parameters can be used to define *a posteriori* a fragility curve depending on this parameter, averaging over the other ones:

$$p_n(PGA) = \mathbb{E}[p_n(\boldsymbol{X})|PGA]. \tag{15}$$

In practice, to obtain numerically the corresponding estimated and reference probabilities, we use k-means algorithm, and divide the database into K groups $(I_1, \ldots, I_K)$ depending on their PGA (resp. on their L, etc.), then compute p_k^{est} and p_k^{ref} as:

$$\begin{array}{rcl} p_k^{est} & = & \frac{1}{n_k} \sum_{i \in I_k} p_n(X_i), \\ p_k^{ref} & = & \frac{1}{n_k} \#\left\{i \in I_k | l_i = 1\right\}, \end{array} \qquad \text{with} \quad n_k = \#I_k. \tag{16}$$

Figures 2 and 3 show two examples of such curves, using PGA or L ; $p_n(\boldsymbol{X})$ is computed using a linear SVM classifier in $\mathbb{R}^4$ with $n = 100$ or $n = 1000$ simulations. In this case, twenty test cases (corresponding to twenty pairs of starting points for the active learning algorithm) are shown in a single figure. The distance between the reference and estimated curves is small in all cases, even with $n = 100$ labeled instances.

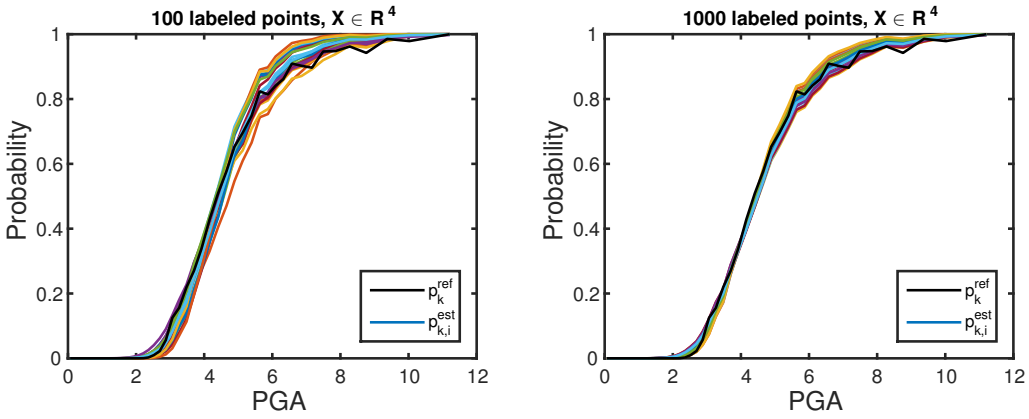

Figure 2: Reference and estimated fragility curves as a function of PGA, using (a) $n = 100$ and (b) $n = 1000$ labeled points [1].

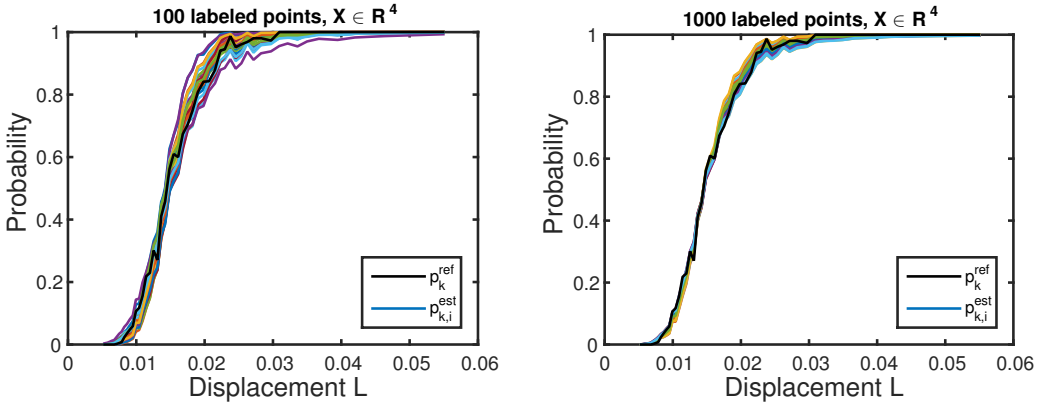

Figure 3: Reference and estimated fragility curves as a function of L, using (a) $n = 100$ and (b) $n = 1000$ labeled points [1].

2.2 ANN Metamodel

A computationally efficient methodology for the application of Artificial Neural Networks (ANN) to characterize the IMs-DM relation is proposed, from the selection of the most relevant IMs to the quantification of ANN prediction uncertainties. Most existing works take subjective choices of the IMs as inputs of metamodels according to their expertise (e.g., PGA or PGA with other IMs). One IM is obviously not sufficient to represent the seismic ground motion. More systematic approaches are proposed in [17, 20] to guide the selection of IMs. Here, different sets of IMs are selected to train ANNs in [17] and the performances of the different sets of IMs are analyzed with respect to their corresponding ANNs median training errors.

It is difficult to directly use stochastic ground motions to construct the metamodels, because the high-dimensionality of the inputs of such metamodels requires a very large size of training data to accurately approximate the input-output relation [25]. An alternative is to use seismic IMs as inputs of the metamodels to represent ground motions. Various functional models based on the calibration of IMs-DM relation have been proposed [37, 38, 39]. According to these works, a nonlinear regression metamodel seems more suitable to provide adequate nonlinearity in the IMs-DM relation. However, with this approach, the simplification of the continuous stochastic ground motion by a small set of IMs may not allow to describe all the random variability in the earthquake motion [10]. Therefore, it cannot ensure the performance of the metamodels.

The following aspects are addressed here:

1. Implementation of an efficient algorithm to select IMs as inputs of the ANN. The most relevant IMs are selected with a forward selection approach based on semi-partial correlation coefficients;

2. Quantification and investigation of the ANN prediction uncertainty computed with the delta method. It consists of an aleatory component from the simplification of the seismic inputs and an epistemic model uncertainty from the limited size of the training data. The aleatory component is integrated in the computation of fragility curves, whereas the epistemic component provides the confidence intervals;
3. Computation of fragility curves with Monte Carlo method and verification of the validity of the log-normal assumption. This methodology is applied to estimate the probability of failure of an electrical cabinet in a reactor building studied in the framework of the KARISMA benchmark.

The uncertainty in the metamodel predictions is also investigated. The ANN prediction uncertainty is considered to be epistemic in [40] to quantify the impact of the size of the used data. The prediction uncertainty is determined by the bootstrap approach, in which retrainings of ANNs are necessary, and it provides confidence intervals of fragility curves. On the contrary, other works integrate the metamodel uncertainty completely into $P_f(\alpha)$ by modeling the standard deviation (Std) of the residual with a dual metamodel (quadratic response surface, HDMR or Kriging) [25, 11, 15, 41]. The residual is sampled from a corresponding normal distribution, and it is added to the mean structural DM predicted by the primal metamodel. With this approach, the residual is an aleatory uncertainty, and the influence of the size of the training data is not accounted for. In addition, the number of FEM simulations required by the dual metamodel approach can be very large, because a number of FEM simulations should be performed *at every design point* with different stochastic motions to obtain the Std. Therefore, it may not be applicable to a very complex structure such as NPP. In this paper, a clearer insight of the ANN prediction uncertainty computed with the delta method is provided: it consists of an aleatory component from the simplification of the seismic inputs and an epistemic uncertainty due to the paucity of the training data. The former is considered in the computation of $P_f(\alpha)$, whereas the latter is used in the estimation of confidence intervals.

Among various types of metamodels, ANNs are chosen due to their adequate nonlinearity and their excellent universal approximation capability for continuous bounded functions [42, 43] (e.g. compared to polynomial response surfaces). Firstly, rather than a classification model like a SVM classifier, which returns only binary failed or survived information for the conditions of structures, an ANN regression model provides predictive structural responses and offers more flexibility for the fragility analysis. Furthermore, the applicability of the ANN does not depend on the probability distribution of input data, so it is a versatile model with a very wide domain of application. Finally, a metamodel based on ANN is a regression rather than an interpolation model. If representative seismic IMs are used to characterize the continuous seismic motions as inputs of the metamodel, the IMs cannot fully represent the seismic randomness and this introduces a residual term. However, an interpolation model predicts identical outputs as the original ground motions for the training data: it may thus overfit the input-output relation. This point is addressed in what follows.

2.2.1 Simulation-based Fragility Analysis

A simulation-based fragility analysis is composed of 3 main steps:

1. Structure modeling. This step consists in establishing a set of mathematical partial differential equations to describe the mechanical behavior of the underlying model.
2. Numerical simulation and calculation of the DM. Numerical simulations are performed to propagate the uncertainties and to compute the DM. FEM is the most widely used numerical resolution method.
3. Computation of the conditional probability of failure of the structure. This step is realized by applying a statistical analysis to the IM-DM data cloud (α, y) computed from the numerical simulation results.

The global procedure for the estimation of the fragility curves with ANNs is illustrated in Figure 4 [44]. The basic stages are:

1. Preparation of data set by performing FEM simulations;
2. Feature selection to extract the most important IMs as inputs of the ANN;
3. ANN training and validation;

4. ANN uncertainty quantification;
5. Computation of fragility curves with ANN simulation results.

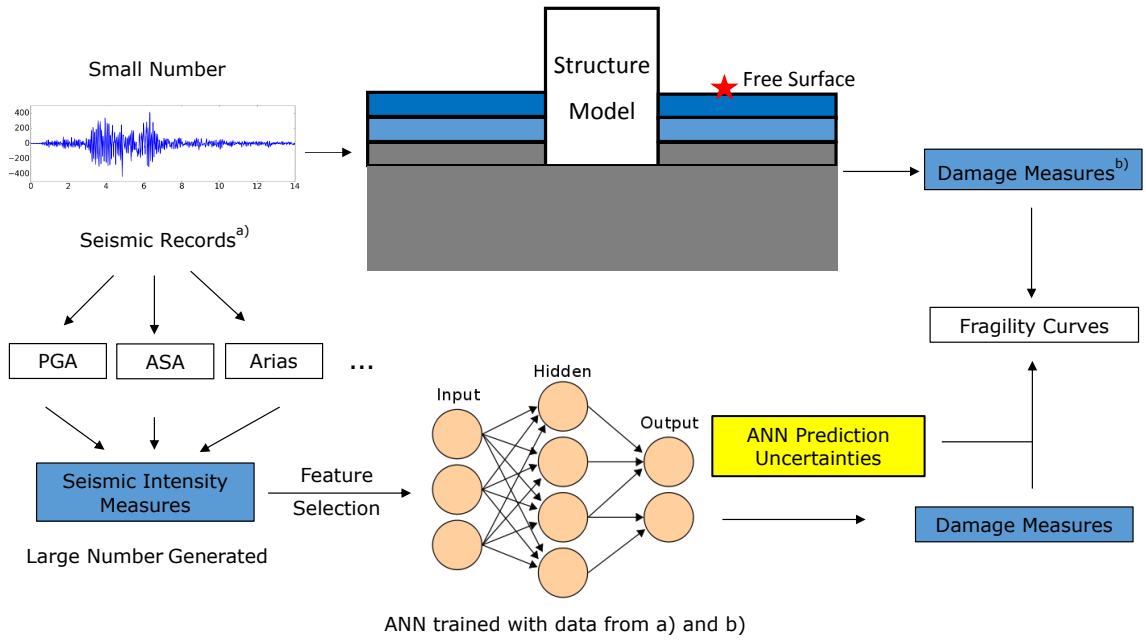

Figure 4: Work flow for the computation of fragility curves with ANN

The constriction of the ANN requires conducting a series of numerical simulations with the FEM. The Soil-Structure Interaction (SSI) should be considered to offer a best estimate of the structural response. The number of simulations is thus limited due to the computational complexity of the FEM analysis, with the presence of the SSI. The basic working flow is divided into the following 5 steps illustrated in Figure 4:

1. Generation of synthetic seismic motions at the bedrock. This can be realized by generating a set of seismic motions compatible with the spectral acceleration predicted by the Ground Motion Prediction Equations (GMPEs).
2. Convolution of the bedrock accelerations to the free surface. The convolution is performed using a 1D column of soil with the consideration of soil degradation. The degradation of the soil during the earthquake is accounted for by the Equivalent Linear Method (ELM) based on the 1D soil column [45].
3. After the convolution, surface ground motions and their corresponding degraded soil profiles are obtained. The ground motions obtained on the free surface are coherent with the site-specific degraded soil profiles. The latter is utilized as the input of the SSI analysis, whereas IMs of the ground motions on the free surface can be extracted.
4. SSI analysis is conducted and structural response time histories can be thus obtained.
5. The DMs are computed by the post-processing of the structural response time histories.

Consequently, the data set IMs-DM is available for the feature selection and further for the construction of the ANN metamodel.

Mechanical model The mechanical model to compute the DM of a structure or a critical component can be described as

$$y = f(a(t)) \tag{17}$$

where $a(t)$ represents the seismic ground acceleration. The resolution of Eq. 17 is usually time-consuming, especially when the structural model is very complex. In this way, one needs to resort to the metamodel to reduce the computational cost of the numerical simulations.

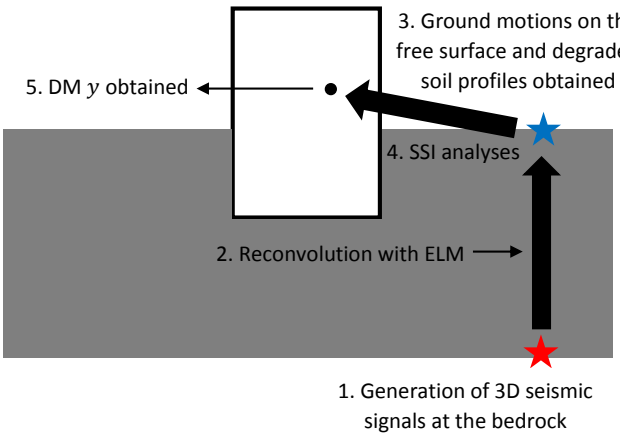

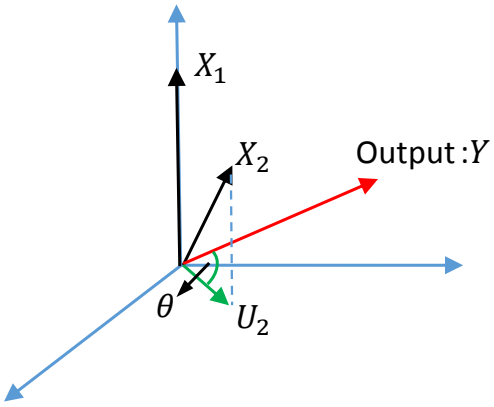

Figure 5: Work flow of FEM simulations (left) and computation of SPCC – $\cos(\theta)$ (right)

Metamodel In this paper, a metamodel established for IMs-DM relation is desired. It is used to replace the mechanical model in order to improve the computational efficiency:

$$\hat{y} = \hat{f}(\mathrm{IM}_1, \mathrm{IM}_2, ..., \mathrm{IM}_k) \tag{18}$$

where the symbol '$\wedge$' denotes the results calculated from the metamodel. The regression of the metamodel leads to a reduction of the variability in the metamodel prediction: $y = \hat{y} + \varepsilon$. The existence of the residual ε not only comes from the lack-of-fit of the metamodel, but also has more specific interpretations:

1. The metamodel cannot show sufficient nonlinearity to replace the mechanical model. The residual value can be very high if a linear metamodel is wrongly selected to substitute a nonlinear mechanical model.
2. IMs are adopted to represent the inherent randomness of ground motions $a(t)$, which gives rise to a loss of information in the input variables. Different ground motion time histories with the same set of IM values lead to different structural responses, in contrast to a deterministic response predicted by the metamodel. Consequently, ε should be present for the training data in the metamodeling process. That is also the main reason why a nonlinear regression model like ANN is preferred, rather than an exact interpolation model, such as Kriging with classical kernels (Gaussian kernel, Matern kernel, etc).
3. The number of the training data for the development of the metamodel is usually limited due to the computational cost of FEM simulations.

These facts show the necessity of the quantification of the metamodel prediction uncertainty, in order to provide reliable applications of metamodels to critical structures such as NPPs.

Both methods, Monte Carlo simulation and linear regression, can be used to compute fragility curves once the ANN metamodel constructed.

Monte Carlo (MC) method In this method, N seismic records with the same IM level α are collected. Structural analyses for all N seismic motions are performed, and the probability of failure for the seismic IM level α is calculated as:

$$p_{\mathrm{MC}}(\alpha) = \frac{1}{N}\sum_{i=1}^{N} 1[y_{\mathrm{crit}} - y^i(\alpha) < 0] \tag{19}$$

where $1[y_{\mathrm{crit}} - y^i(\alpha) < 0]$ equals 1 if $y_{\mathrm{crit}} - y^i(\alpha) < 0$, otherwise it equals 0. In particular, the pointwise MC method serves to confirm the validity of the log-normal assumption for fragility curves.

Regression method with log-normal assumption The log-normal assumption is commonly adopted to compute the conditional probability of failure. The regression method (Reg), or 'cloud analysis', is based on the linear regression of the data cloud (α, y) in the log-log space [46, 37, 47]:

$$\ln y = c \ln \alpha + \ln b + \varepsilon \tag{20}$$

where b and c are regression parameters determined from the data cloud ($\ln \alpha$, $\ln y$), and the residual ε follows a normal distribution $\mathcal{N}(0, \beta^2_{R|IM})$. $\beta_{R|IM}$ is calculated as:

$$\beta_{R|IM} = \sqrt{\frac{\sum_{i=0}^{N}(\varepsilon^i - \bar{\varepsilon})^2}{N-2}} \tag{21}$$

in which $\bar{\varepsilon}$ is the mean of the regression residuals and N denotes the size of the data (α, y). The conditional probability of failure can be, thus, calculated:

$$p_f(\alpha) = \mathbf{\Phi}\left(\frac{\ln b\alpha^c - \ln y_{\mathrm{crit}}}{\beta_{R|IM}}\right) \tag{22}$$

where $\mathbf{\Phi}(\cdot)$ is the cumulative distribution function of the standard normal distribution $\mathcal{N}(0, 1)$.

2.2.2 ANN Training and Validation

The structure of a classical, three-layer, feed-forward ANN is illustrated in Figure 6. Mathematically, this ANN consists of activation functions (linear functions, and nonlinear tanh functions) and a set of model parameters. The model parameters are the ANN weights w and biases b, which are adjusted by training to minimize a cost function. The cost function computes the difference between the ANN predictions $\hat{y}$ and the targets y (e.g. FEM simulation results), summed over every training example i. For simplicity of notation, in this paper, w is used to represent all parameters of the ANNs, including weights and biases:

$$E(x;w) = \frac{1}{2}\sum_{i=1}^{N}(\hat{y}^i(x;w) - y^i)^2 \tag{23}$$

where $E(x;w)$ denotes the cost function which the ANN aims to minimize, N is the total number of ANN training examples, and x is the ANN input vector.

The ANN is trained based on the gradient vector g, which can be computed efficiently by the back-propagation algorithm [42, 48]:

$$g = \frac{\partial E(x;w)}{\partial w} \tag{24}$$

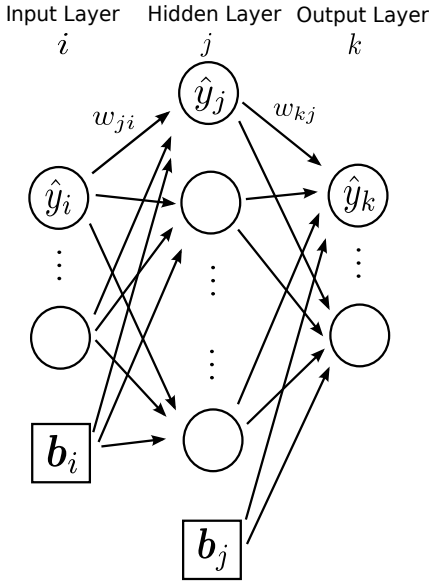

Figure 6: A multiple-layer perceptron model

For the ANN training, the available data set is divided into 3 independent subsets:

1. Training subset (e.g., 60% of the total data), which is used to determine the optimal weighting parameters w^* that minimize the cost function of the ANN model.
2. Validation subset (e.g., 20% of the total data), which supervises the training process. The ANN training is stopped when the validation error reaches its minimum to avoid overfitting [42, 49]. This strategy is called *early stopping*.
3. Test subset (e.g., 20% of the total data), which is independent of the training and validation subsets. The test subset is not used in the ANN training, but used afterwards to evaluate the generalization capacity of a trained ANN metamodel.

The ANN is suggested to be trained with IMs-DMs in log-log space to facilitate the consideration of the ANN uncertainties into the fragility curves. The performance of the ANN can be evaluated by the root-mean-square error (RMSE). Once trained and validated, the ANN substitutes the FEM model to accelerate the computation process.

2.2.3 ANN Uncertainty Quantification

Besides the ANN deterministic prediction $\hat{y}$, the confidence interval (CI) of this prediction can be also estimated. The main methods to evaluate the prediction intervals (PIs) of ANNs are the bootstrap method, the Bayesian approach and the delta method [50]. The delta method is adopted in this study due to its computational efficiency because it does not require repeated trainings of the ANNs with the bootstrap resampling[51]. Assuming a normal distribution of the ANN training error, this method relies on the linear Taylor expansion of the ANN model and estimates the PIs of the corresponding linear model [51, 52, 53]. In this way, the Hessian matrix of the ANN is approximated by the product of the Jacobian matrices. Mathematically, the PIs are computed with the Std of the ANN training error σ_{ANN} and the gradient vector h:

$$h^i = \frac{\partial \hat{y}^i}{\partial w} = \frac{\partial \hat{y}^i}{\partial E(x;w)} \frac{\partial E(x;w)}{\partial w} = \frac{g}{\hat{y}^i - y^i} \tag{25}$$

The Jacobian matrix J of the ANN training data is, hence, constructed as

$$J = \begin{bmatrix} h^1 & h^2 & \cdots & h^i & \cdots & h^N \end{bmatrix} \tag{26}$$

where J is a $Q \times N$ matrix, with N the number of the ANN training examples and Q the number of the weighting parameters in the ANN. Consequently, the prediction uncertainties of ANNs are calculated as

$$s^2 = \sigma^2_{\mathrm{ANN}} + \sigma^2_{\mathrm{ANN}} h^\top_{\mathrm{test}} (JJ^\top)^{-1} h_{\mathrm{test}} \tag{27}$$

where s denotes the Std of the ANN predictions.

The source of the ANN prediction uncertainty comes from two aspects:

1. The selected IMs cannot completely represent the variability of the ground motion. This eventually reduces the variability of the output;
2. The ANN accuracy due to the limited size of data to train ANNs.

It is the statistical uncertainty linked to the ANN model. Let us return to the two components in s^2: the first fixed part (σ^2_{ANN}) represents the ANN training error, and the second part ($\sigma^2_{\mathrm{ANN,stat}} \triangleq \sigma^2_{\mathrm{ANN}} h^T_{\mathrm{test}} (JJ^T)^{-1} h_{\mathrm{test}}$) depends on the training and the test data.

1. The first term σ^2_{ANN} estimates the difference between the FEM simulation results and the predictions of the ANN. Given that a nonlinear regression returns a regular hyper-surface in a high dimensional space, the predictions of the ANN show always less variability than the original FEM data. This phenomenon is mainly due to the loss of the inherent seismic randomness in the input variables, so that the nature of σ^2_{ANN} can be regarded as the aleatory uncertainty not explained by the ANN input parameters.
2. The second term $\sigma^2_{\mathrm{ANN,stat}}$ is the statistical uncertainty linked to the limited data used to train and test the ANNs. The information of the training data is included in the J matrix and h_{test} incorporates the influence of the test data. It is thus considered as the epistemic uncertainty, and it provides the confidence intervals of the fragility curves.

These two aspects are illustrated with a simple case study in Figure 7 and Figure 8 for 80 sparse training data $y = \sin(x) + z$, with $z \sim \mathcal{N}(0, 0.1^2)$. An ANN is trained with (x, y) where z is assumed to be the unidentified input. No training data are generated near $x = 3$, for the purpose of checking the property of $\sigma_{\mathrm{ANN,stat}}$. (b) ANN is trained, with $\sigma_{\mathrm{ANN}} = 0.0931$, close to the Std of z. The ANN is then tested on 100 uniformly regenerated data. (c) $\sigma_{\mathrm{ANN,stat}}$ with a peak near $x = 3$, where no training data exist. It can be concluded that $\sigma_{\mathrm{ANN,stat}}$ captures the scarcity of the training data. In fact, σ_{ANN} should have contained also an epistemic uncertainty contribution from the insufficient nonlinearity of the ANN. However, the high flexibility of the ANN architecture offers an universal approximation capacity to continuous bounded functions [43]. If the number of the hidden layer units is correctly determined, the error from the ANN nonlinearity can be considered less important compared to the aleatory randomness neglected in its inputs. This can be observed from Figure 7: in spite of the existence of the unidentified input z, the ANN regression curve stays very close to $y = \sin(x)$ curve in the training data region. Consequently, this epistemic contribution is assumed negligible in this study. Next section presents the computation of fragility curves with the consideration of these two uncertainties.

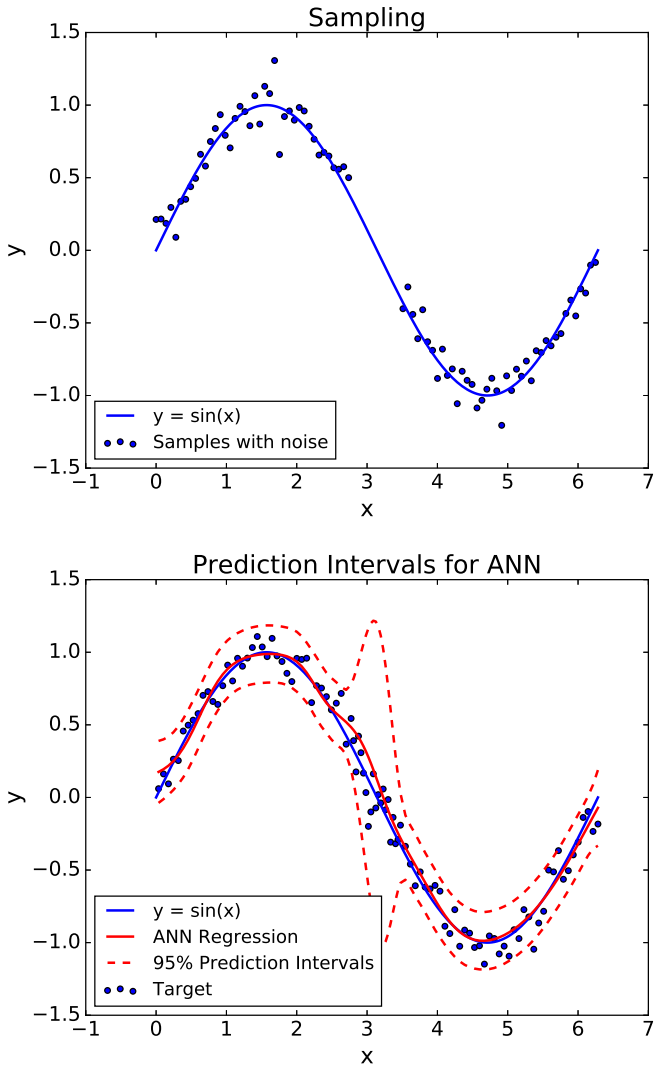

Figure 7: ANN Training data (left) and ANN Test results (right)

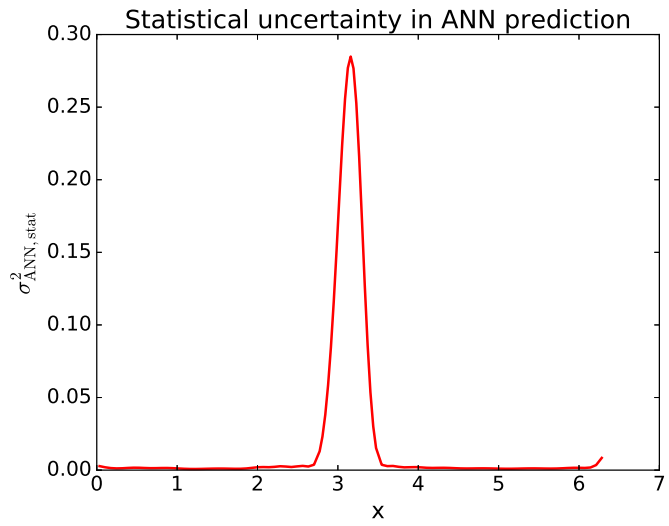

Figure 8: ANN statistical uncertainty

2.2.4 Case Study: KARISMA benchmark

In 2007, the Japanese Kashiwazaki-Kariwa (K-K) NPP was affected by the Niigataken-Chuetsu-Oki Earthquake (NCOE) with a magnitude $M_w = 6.6$ and an epicenter distance of 16 km. The structure of the K-K NPP is shown in Figure 2.2.4. In this paper, we are interested in the reliability of a hypothetical electrical cabinet located on the fifth floor of the Unit 7 reactor building of the NPP (Figure 2.2.4). The finite element model for the Unit 7 consists of 92,000 degrees of freedom with 10,700 nodes and 15,600 elements, including bar, beam, and different shell elements. The constitutive law of the materials is considered as linear. The NPP model is embedded 23 meters in the soil, which is accounted for in the SSI analysis. The structural analyses are carried out with Code_Aster, a finite element analysis open-source software developed by EDF group [54], while the soil part is solved with MISS based on the Boundary Element Method (BEM) [55].

FEM analyses are performed with 100 triplets of 3D synthetic ground motions are generated at the bedrock with $Vs_{30} = 720\ \mathrm{m/s}$ and used for the uncertainty propagation. Given the NCOE scenario, the generation of the synthetic ground motions are based on scenario spectra predicted by the Campbell-Bozorgnia 2008 (C&B 2008) GMPE [56]. In order to obtain sufficient failure cases for the fragility analysis, the synthetic seismic motions at the bedrock are scaled with a factor of *three*. After analyses with ELM, 100 triplets of ground motions on the free surface and 100 degraded soil profiles are obtained.

The impedances of the soil and the seismic forces should have been computed for each soil profile using BEM. However, the high complexity of the embedded foundation makes it hard to achieve: it takes 24 hours to run the BEM simulation for one soil profile. In order to reduce the computational cost, the 3D seismic signals at the bedrock are regrouped into four soil classes according to their PGA values: i. PGA∈[0, 0.5g) ii. PGA∈[0.5g, 1.0g) iii. PGA∈[1.0g, 1.5g) iv. PGA∈[1.5g, +∞). The degraded soil profiles are averaged within each class and four soil profiles are obtained to represent four different degradation levels. The SSI analyses are performed with the 100 ground motions on the free surface, as well as the impedances and seismic forces calculated from the four soil profiles, to compute the floor accelerations of the K-K NPP.

Anchorage failure of the electrical cabinet is considered in this study. The capacity is given by the floor spectral acceleration of the anchorage point around 4Hz, the assumed natural frequency of the cabinet. The maximum value of the floor spectral accelerations in the two horizontal directions, integrated over a frequency interval around 4Hz to account for the uncertainty, is defined as the DM y:

$$y = \max_{i=X,Y} \int_{3.5}^{4.5} S^e_{a,i}(f)\mathrm{d}f \tag{28}$$

where $S^e_{a,i}$ denotes the spectral acceleration of the electrical equipment in the i-th direction. Figure 2.2.4 shows the 100 calculated DMs as a function of the geometric mean of the PGAs of the horizontal seismic motions on the free surface.

The 100 IMs-DM obtained from FEM simulations can be used for the construction and the training of the ANN metamodel. 8 classical IMs are chosen as candidates for the inputs of the ANN metamodel. The 8 IMs include the commonly used seismic intensity indicators PGA, PGV, PGD, $\mathrm{PS}_a(f_0)$, CAV, Arias intensity I_A, as well as the predominant period T_p used in [57] and the ASA proposed in [58]. These IMs are presented in detail in Table 1. The geometric means of IMs in the two horizontal directions are used as scalar IMs for 3D ground motions. The integration domain of the ASA is slightly modified compared to its initial definition in [58], to consider the uncertainty on the natural frequency of the electrical cabinet.

The correlation coefficients ρ between the eight IMs and the DM defined by 28 are listed in Table 2. It can be observed that, among all the eight chosen IMs, ASA is the most relevant IM to the DM, whereas there is a very weak correlation for T_p.

The statistical distributions of the eight selected IMs are examined to check their log-normality. The eight proposed IMs are normalized and compared to $\mathcal{N}(0,1)$. The normalization is realized by:

$$\alpha_{\mathrm{Norm}} = \frac{\ln\alpha - \mu_{\ln\alpha}}{\sigma_{\ln\alpha}} \tag{29}$$

where $\mu_{\ln\alpha}$ and $\sigma_{\ln\alpha}$ denote the mean and the Std of $\ln\alpha$, respectively. For simplicity of illustration, the probability plots of three IMs (PGA, ASA and I_A) are shown in Figure 10. Besides, the values of the

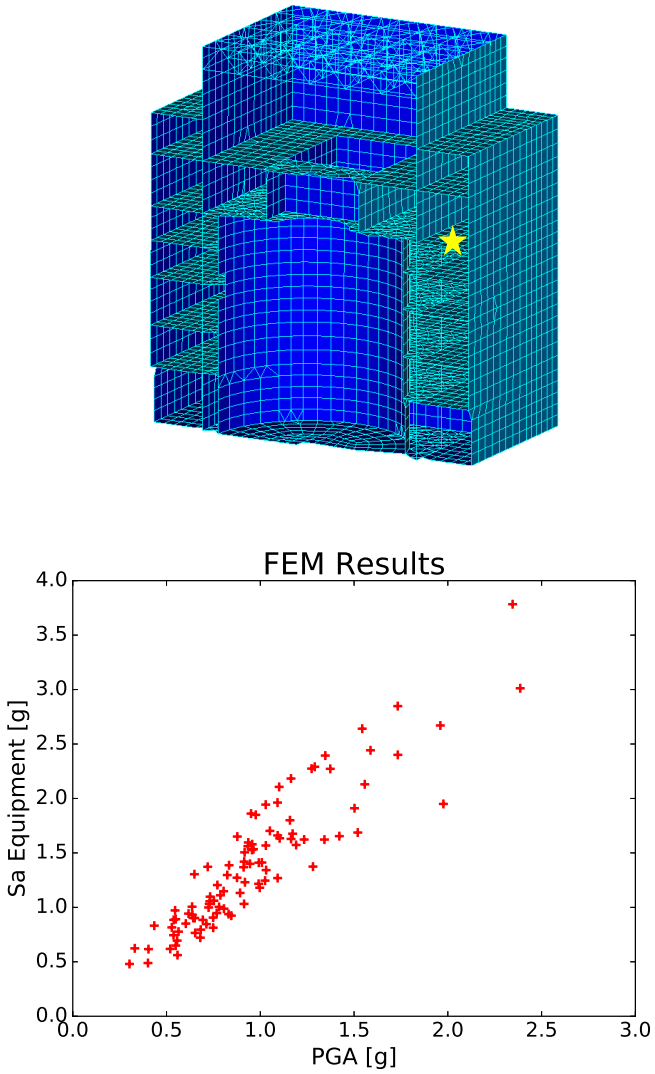

Figure 9: Location of the electrical cabinet in the K-K model, indicated by the star symbol (left) and point cloud of DMs calculated with FEM (right)

Table 1: Definitions of classical seismic intensity measures. Legend: PGA (peak ground acceleration), PGV (peak ground velocity), PGD (peak ground displacement), $\mathrm{PS}_a(f_0)$ (pseudo-spectral acceleration), ASA (average spectral acceleration), T_p (predominant period), CAV (cumulative absolute velocity), I_A (Arias intensity)

Intensity Measures	Definitions	Comments
PGA	$\max\|a(t)\|$	$a(t)$: seismic acceleration
PGV	$\max\|v(t)\|$	$v(t)$: seismic velocity
PGD	$\max\|u(t)\|$	$u(t)$: seismic displacement
$\mathrm{PS}_a(f_0)$	Spectral acceleration	f_0=4Hz, damping 5%
ASA	$\int_{3.5}^{4.5}\mathrm{PS}_a(f)\mathrm{d}f$	f: frequency
T_p	$argmax_T\mathrm{PS}_a(1/T)$	$T=1/f$
CAV	$\int_0^{t_{\max}}\|a(t)\|\mathrm{d}t$	$t_{\max}$: total seismic duration
I_A	$\frac{\pi}{2g}\int_0^{t_{\max}}a(t)^2\mathrm{d}t$	g = 9.81$\mathrm{m/s^2}$

Table 2: Correlation coefficients between IMs and DM

IMs	PGA	PGV	PGD	PS_a	ASA	T_p	CAV	I_A
ρ	0.913	0.693	0.420	0.920	0.950	0.093	0.889	0.890

coefficients of determination R^2 of the probability plots are given in Table 3, for all the eight IMs: the closer to the log-normal distribution the IM is, the closer to 1 the value of R^2 will be. It can be concluded that it is reasonable to apply the log-normal distribution model to all eight IMs.

This verification is performed because: i) For the selection of the subset of IMs, the Cholesky factorization is executed on the covariance matrix of Gaussian random variables (RVs). As a result, if the IMs follow log-normal distributions, the Cholesky factorization can be directly applied to $\ln(\mathrm{IMs})$. ii) For the generation of IMs in the ANN simulation part, one needs to know the marginal distribution of the IMs to be generated. In this way, it can be confirmed that the marginal distributions of the IMs are effectively log-normal. If the IMs are not log-normally distributed, an additional Nataf transformation [59] should be carried out, to transform arbitrary RVs to Gaussian RVs.

Table 3: Coefficients of determination of the probability plots

IMs	PGA	PGV	PGD	PS_a	ASA	T_p	CAV	I_A
R^2	0.9877	0.9970	0.9915	0.9866	0.9896	0.9823	0.9912	0.9913

The ANN is trained with two inputs (ASA and I_A), four hidden layer nodes and one output, which is computed according to Eq. 28. The trained ANN is used for all runs of ANN simulations. Point clouds and fragility curves will be plotted with ASA, which is the most efficient IM in this study.

Training results Training based on the back-propagation algorithm is carried out with the ANN structure determined by the filter approach. The ANN toolbox used in this study is an open-source python package 'Neurolab' with the self-implemented delta method for the quantification of ANN prediction uncertainties. The is again divided into 2 subsets: 60 data for training and 20 data for validation. Early stopping is applied on the validation set to avoid overfitting. The generalization capacity of the ANN is examined on the 20 test data. The ANN is trained in *log-log space*. The results of the ANN training, as well as the point clouds of the ANN outputs $\hat{y}$ of the test data are shown in Figure 11 and Figure 12. From Figure 11, one can conclude that the training results are satisfactory. Most of the results in the 'prediction-target' space are located in the neighborhood of the dashed diagonal line. The ANN prediction results for the test data set in Figure 12 reveal a globally satisfactory prediction quality: the ANN predictions remain coherent with the FEM results. In fact, with a regression model like ANN, it is not possible to obtain the exact prediction results. In addition, it has to be pointed out that the dispersion of the ANN predictions is reduced compared to the FEM results. This is due to the loss of the aleatory uncertainty by reducing ground motions to two IMs in the ANN metamodeling. The underestimated variability in the ANN predictions will reduce the uncertainty in the fragility curve. The histogram of the normalized ANN training residuals is plotted in Figure 12. It can be observed that its distribution is close to $\mathcal{N}(0,1)$, so that the assumption of normality of the ANN residuals in the delta method can be considered reasonable in this study.

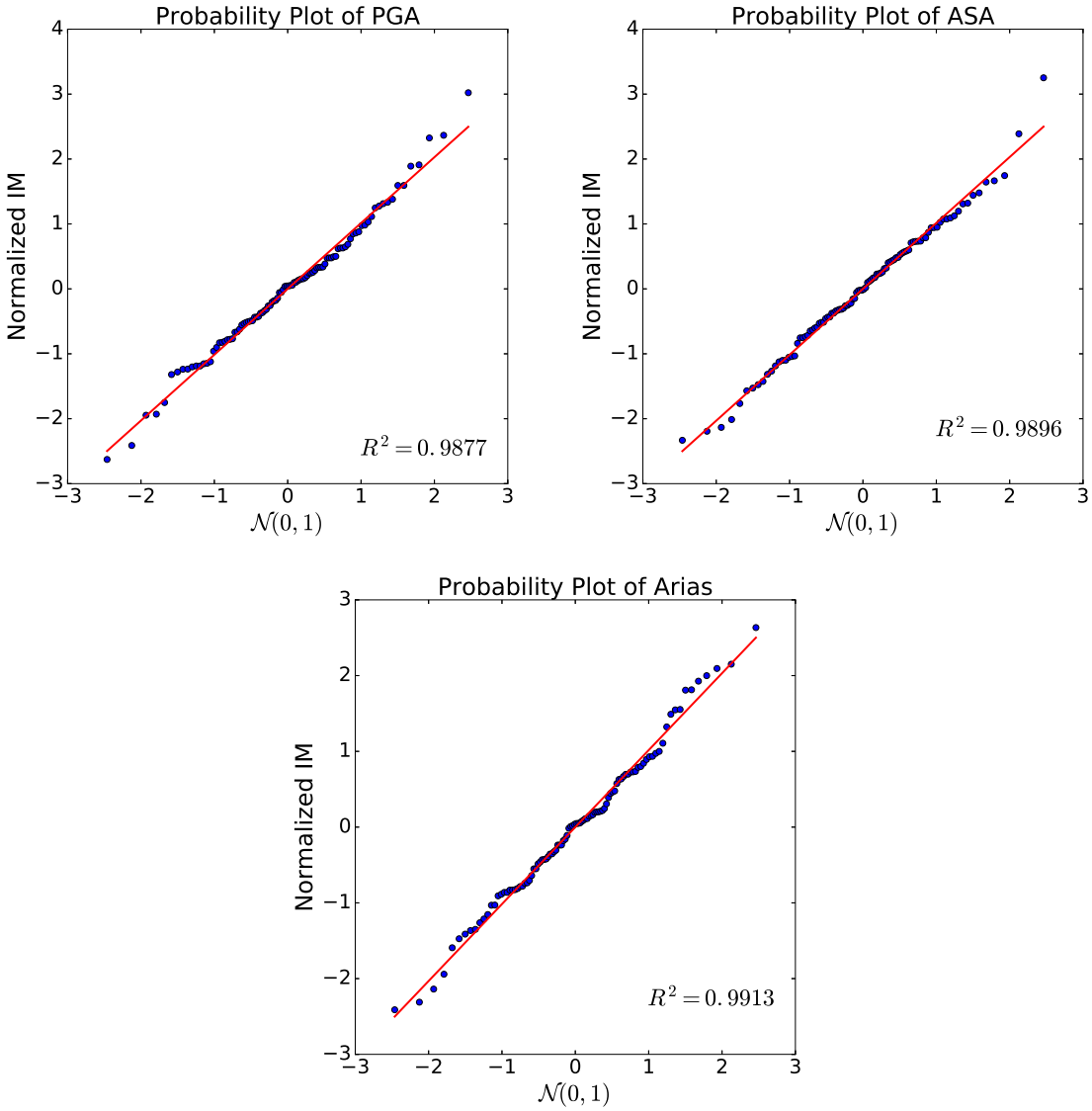

Figure 10: Probability plots for PGA, ASA and I_A to check their log-normality

Comparison with other metamodels The training results of the ANN are compared with those of other metamodels, including Kriging with Gaussian kernel (an interpolation model), Kriging with Gaussian and White noise kernel (a regression model) and quadratic response surface. The metamodels are constructed with 80 T-CV data and tested on 20 test data, using the python toolbox scikit-learn. The RMSE between metamodel predictions and FEM outputs is used to evaluate the accuracy of the different metamodels. The seismic IMs used are ASA and I_A, the same used for the ANN. The results are reported in Table 4.

Table 4: Training and test results for different metamodels

Model	RMSE Training (80 data)	RMSE Test (20 data)
ANN	0.141	0.135
Kriging interpolation (Gaussian kernel)	0	0.43
Kriging regression (Gaussian+White noise kernel)	0.153	0.145
Quadratic response surface	0.151	0.151

Several conclusions can be drawn from Table 4:

1. Kriging interpolation is not an appropriate metamodel for this study, since the test error is much larger than other models. The reason is the zero residual in the training of Kriging overfits the

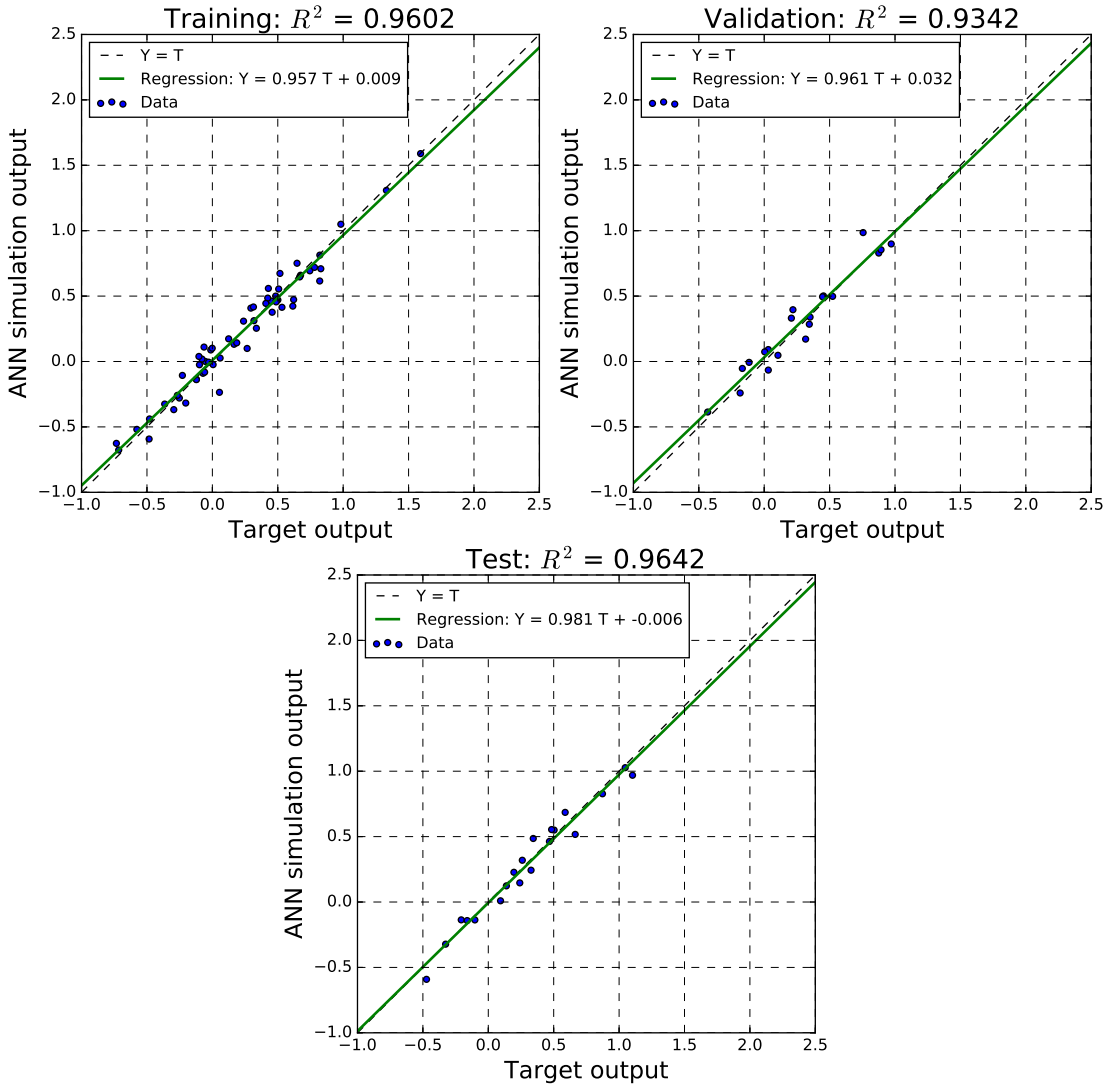

Figure 11: Training set, validation set and test set

model. The generalization capability of the interpolation Kriging model is thus very limited with the underlying data;

2. Once the residual is present in the training data of the Kriging regression, the performance of the Kriging is largely improved;
3. Quadratic response surface offers less nonlinearity than ANN, which is why its errors are larger;
4. Overall, ANN shows slightly better performance than other considered metamodels.

Fragility curves After being trained, the ANN can be used to carry out fast-running simulations. For this purpose, a large number of seismic IMs have to be generated to represent the seismic motions. In this paper, the following statistical properties of the log-normal distributions of ASA and I_A are obtained from the 100 triplets of seismic signals on the free surface (Table 5).

With the large number of simulation results provided by the ANN, both methods presented above can be applied for the computation of fragility curves.

Table 5: Statistics of ASA and I_A on the free surface

IM	Median	Log. standard deviation	ρ (ASA-I_A)
ASA [g]	2.28	0.417	0.846
I_A [m/s]	13.13	0.842	0.846

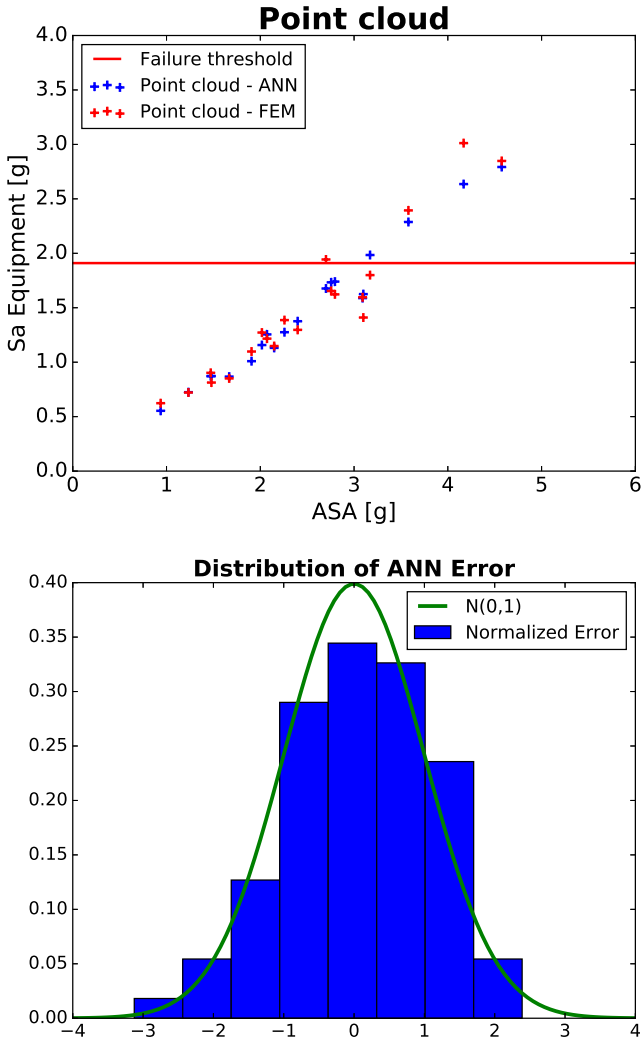

Figure 12: ANN test point cloud (left) and distribution of ANN training residuals (right)

For the log-normal based fragility curve, 10,000 ASA-I_A samples are generated with the statistics in Table 5. 10,000 ANN simulations are performed with these generated IMs, and the conditional probability of failure is computed by regression. The computed fragility curve is described by ASA with median capacity 3.32g and uncertainty $\beta_{\text{Total}} = 0.127$, including $\sigma_{\text{ANN}} = 0.094$.

The pointwise fragility analysis is performed by conditional sampling of I_A for a given value of ASA, since a conditional bivariate normal distribution is also normally distributed. In the analysis, the values of ASA are selected in [2.2g, 4.4g] with ΔASA = 0.1g. For every ASA value, 10,000 I_A are generated. Fragility curves computed with both methods are shown in Figure 13.

Regarding the fragility curves, although there exist some differences between the log-normal based fragility curve and the MC estimation, the log-normal curve stays coherent with the pointwise MC curve. The log-normal assumption can be thus confirmed in this study. It is recalled that the source of the confidence intervals comes only from the paucity of the training data of the ANN.

Based on the soil impedances computed by BEM, one single FEM analysis takes $(120.02+66.86)/100 = 1.87$ hours on an Intel Xeon E5-2600V2 CPU of 2.7GHz, which makes it almost unaffordable to run a large number of FEM simulations for the pointwise MC fragility analysis. However, once the ANN metamodel is established, the pointwise MC fragility analysis can be conducted within 0.25 hours. It has to be noticed that the ANN metamodel is constructed from the results of 100 FEM simulations, which means that $132.41 + 120.02 + 66.86 = 319.29$ hours of mechanical simulations are the prerequisites for the ANN metamodel construction.

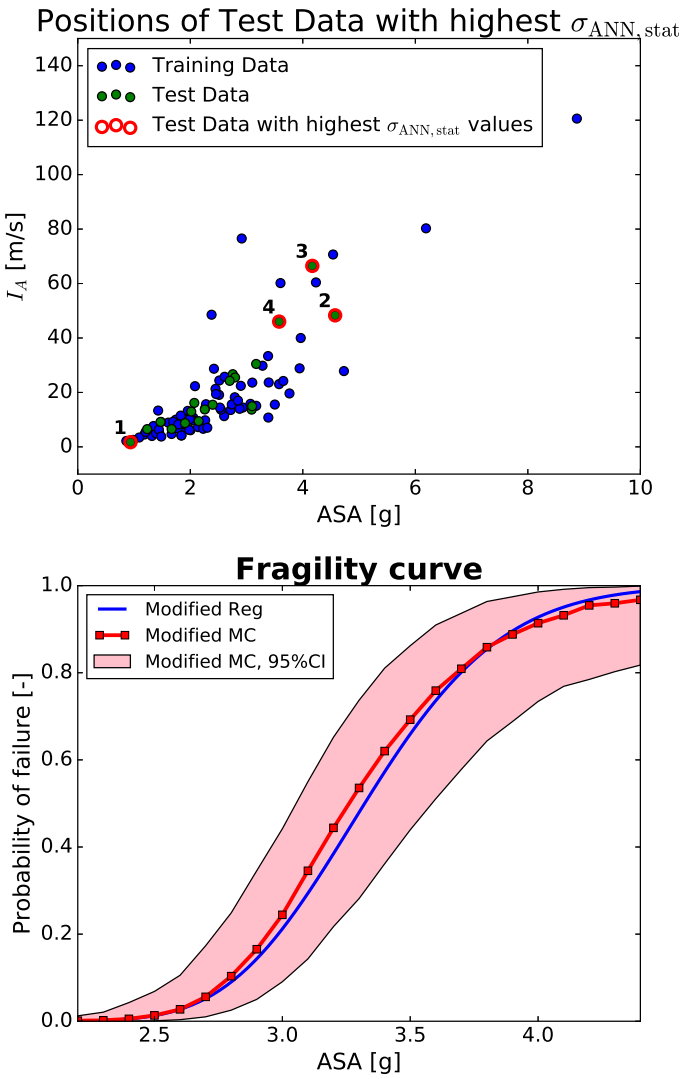

Figure 13: Positions of test data with highest $\sigma_{\mathrm{ANN,stat}}$ (left) and fragility curves with ANN (right)

3 Metamodels for Tsunami

The metamodel aims at approximating the tsunami-induced Sea Surface Elevation SSE as a function of the source parameters $\boldsymbol{\theta}$. The selected technique is the kriging approach [60, 61] which enables to learn in a nonparametric manner the statistical link between the scenario parameters and the indicator of tsunami hazard. Basic concepts are briefly described in the following for the scalar case. For a more complete introduction to kriging metamodelling and full derivation of equations, the interested reader can refer to Forrester et al. [60].

3.1 Kriging metamodelling and validation

Let us define $\boldsymbol{\theta}_D$ the design matrix composed of the vectors of source characteristics $\boldsymbol{\theta}$ (i.e. typically of small number $n \sim 100$) so that $\boldsymbol{\theta}_D = (\boldsymbol{\theta}^{(1)}; \boldsymbol{\theta}^{(2)}; ...; \boldsymbol{\theta}^{(n)})$ and $\boldsymbol{H}_D$ the vector of tsunami-induced SSE values, which are calculated using the numerical code so that $\boldsymbol{H}_D = (H^{(1)} = f(\boldsymbol{\theta}^{(1)}); H^{(2)} = f(\boldsymbol{\theta}^{(2)}); ...; H^{(n)} = f(\boldsymbol{\theta}^{(n)}))$.

Under the assumptions underlying the kriging metamodel, the statistical distribution of *H* for a new input vector $\boldsymbol{\theta}^*$ follows a Gaussian distribution conditional on the design matrix $\boldsymbol{\theta}_D$ and of the corresponding results $\boldsymbol{H}_D$ with expected value $\tilde{H}(\boldsymbol{\theta}^*)$ for the new configuration $\boldsymbol{\theta}^*$ given by the kriging mean (using the ordinary kriging equations):

$$\tilde{H}(\boldsymbol{\theta}^*) = \hat{H} + \boldsymbol{r}^\top(\boldsymbol{\theta}^*).\boldsymbol{R}_D^{-1}.(\boldsymbol{H}_D - \mathbf{1}.\hat{H}) \tag{30}$$

where $\hat{H} = (\mathbf{1}^\top.\boldsymbol{R}_D^{-1}.\mathbf{1})^{-1}.(\mathbf{1}^\top.\boldsymbol{R}_D^{-1}.\boldsymbol{H}_D)$ is a constant; $\boldsymbol{r}(\boldsymbol{\theta}^*)$ is the correlation vector between the test candidate $\boldsymbol{\theta}^*$ and the training samples; $\boldsymbol{R}_D$ is the correlation matrix of the training samples $\boldsymbol{\theta}_D$ and $\mathbf{1}$ is the unit vector of size n.

The kriging variance holds as follows:

$$s^2(\boldsymbol{\theta}^*) = \hat{\sigma}^2.(1 - \boldsymbol{r}^\top(\boldsymbol{\theta}^*).\boldsymbol{R}_D^{-1}.\boldsymbol{r}(\boldsymbol{\theta}^*) + \frac{(1 - \mathbf{1}^\top.\boldsymbol{R}_D^{-1} \cdot \boldsymbol{r}(\boldsymbol{\theta}^*))^2}{\mathbf{1}^\top.\boldsymbol{R}_D^{-1}.\mathbf{1}}) \tag{31}$$

with the constant $s^2(\boldsymbol{\theta}^*) = (\boldsymbol{H}_D - \mathbf{1}.\hat{\boldsymbol{H}})^\top.\boldsymbol{R}_D^{-1}.(\boldsymbol{H}_D - \mathbf{1}.\hat{\boldsymbol{H}})^\top/n$.

A key issue is the validation of the approximation i.e. the verification that the statistical emulator can estimate with high accuracy not-yet-seen new input configurations $\boldsymbol{\theta}^*$. This can rely on leave-one-out cross-validation procedures (e.g. [62]) from which the coefficient of determination $\mathcal{Q}_2$ can be computed:

$$R^2 = 1 - \frac{\sum_{i=1}^{n} (H^{(i)} - \tilde{H}^{(i)})^2}{(H^{(i)} - \bar{H})^2} \tag{32}$$

where $H^{(i)}$ corresponds to the i^{th} *H* value (i=1,...,*n*), $\bar{H}$ to the mean, and $\tilde{H}^{(i)}$ to the approximated SSE value using the metamodel. A coefficient R^2 close to 1 indicates that the metamodel is sucessful in matching the observations. A typical threshold of 80% is often used to evaluate the validation quality.

In addition, the metamodel errors related to the use of an approximation (of statistical nature) in place of the true simulator can be modelled via a Gaussian probability distribution with mean corresponds to equation 30 and variance to equation 31. Along the propagation related to the uncertainties on $\boldsymbol{\theta}$, the metamodel errors can also be accounted for by sampling from the afore-described Gaussian distributions (Roustant et al. [61]: Sect. 4.2).

3.2 Tsunami-induced wave modelling procedure

In this section, we describe the numerical modelling strategy to simulate the tsunami-induced sea surface elevation denoted SSE. Numerical simulations are used to estimate the tsunami-induced SSE based on FUNWAVE-TVD code (see a recent application on the Tohoku-Oki tsunami by Grilli et al. [63]). It uses a Total Variation Diminishing (SSE) shock-capturing algorithm with a hybrid finite-volume and finite-difference scheme to more accurately simulate wave breaking and inundation by turning off dispersive terms (hence solving Non-Linear Shallow Water equations during breaking) once wave breaking

is detected (based on the Froude number of the flow). The code is fully parallelized using the Message Passing Interface (MPI) protocol, using efficient algorithms allowing a substantial acceleration of the computations with the number of computer cores. A coseismic tsunami is assumed to be generated by a sudden static vertical displacement of the seafloor due to slip on a dip-slip fault that ruptured at depth. The rupture is modelled by an elastic dislocation using analytic expressions described by Okada [64]. The coseismic slip is assumed to be spatially uniform on a planar fault centered at a given hypocenter. The source parameters are: epicentral position (longitude and latitude), depth, azimuth, dip and rake angles, average coseismic slip along fault, length and width of fault.

3.3 Case study: Ligurian sea tsunami

In this section, we first provide details on the Ligurian case study and discuss results. These developments initiated in a previous project (ANR Tandem) were used as a basis for NARSIS work on metamodels.

3.3.1 Description of the Ligurian case

The study is focused on the Ligurian sea tsunami (see location in Figure 14) induced by the damaging historical earthquake in 1887. The February, 23^{rd} 1887 earthquake was the largest event reported in the Alps-Liguria region. It induced damages due to ground shaking and the largest coseismic tsunami recorded in the North-West Mediterranean basin [65]. This event occurred in a low deformation rate region, namely the Alps-Ligurian Basin junction, but is associated with some historical earthquakes as indicated in Figure 14 (see also [66, 67] for a more detailed introduction of the regional context). Location, magnitude and fault mechanism responsible for the 1887 event have been discussed for a long time (e.g. [68]). In particular, the magnitude (M_w) range proposed for this event ranges from 6.2 to 6.9 [66]. From local seismotectonic analysis and macroseismic as well as from tsunami historical databases and simulations, Larroque et al. [66] and loualalen et al. [67] proposed that the 1887 Ligurian earthquake occurred along some segments of the Ligurian Faults system (Figure 14, bottom). In the following, we primarily focus on a North dipping fault, which is one of the most plausible scenario [67]. Based on these studies as well as on local tectonic setting, uncertainty ranges are constrained for nine source parameters (Table 6), by assuming that the source parameter' variability is described by a uniform probability law.

Table 6: Uncertainty range of the source and bias parameters in the Ligurian case

Source parameter	Lower bound	Upper bound	Unit	Symbol
longitude	7.78	8.15	°	*Lon*
latitude	43.45	43.92	°	*Lat*
Depth	5	20	km	*Z*
Azimuth	220	260	°	*Azi*
Dip	10	70	°	*Dip*
Rake	70	110	°	*Rake*
Average slip	0.3	2	m	*D*
Length	20	57	km	*L*
Width	10	22	km	*W*

3.3.2 Application and analysis of the simulation results

Given the domain of variation of the different source model parameters (Table 6), three hundred of simulation scenarios were generated (each being associated to a different setting of source parameters' values) using the Latin Hypercube Sampling (LHS) method [69]. The mesh model in spherical coordinates is based on the bathymetry dataset of European Marine Observation and Data Network [70] at a spatial resolution of 0.002° (~ 230 m); see Figure 14. It is composed of more than 2 millions of mesh cells and extends from Marseille to Genova. The computation time cost is of around 0.5-1 hour (for a single model run) using a cluster of 96 computers running in parallel.

Kriging metamodels were constructed by considering the different key locations along the coast (Figure 14). A leave-one-out cross –validation procedure was conducted to confirm the predictability of the different metamodels: this showed R^2 indicator values of at least 85% hence confirming the validity of replacing the long running simulators by these metamodels (Figure 15).

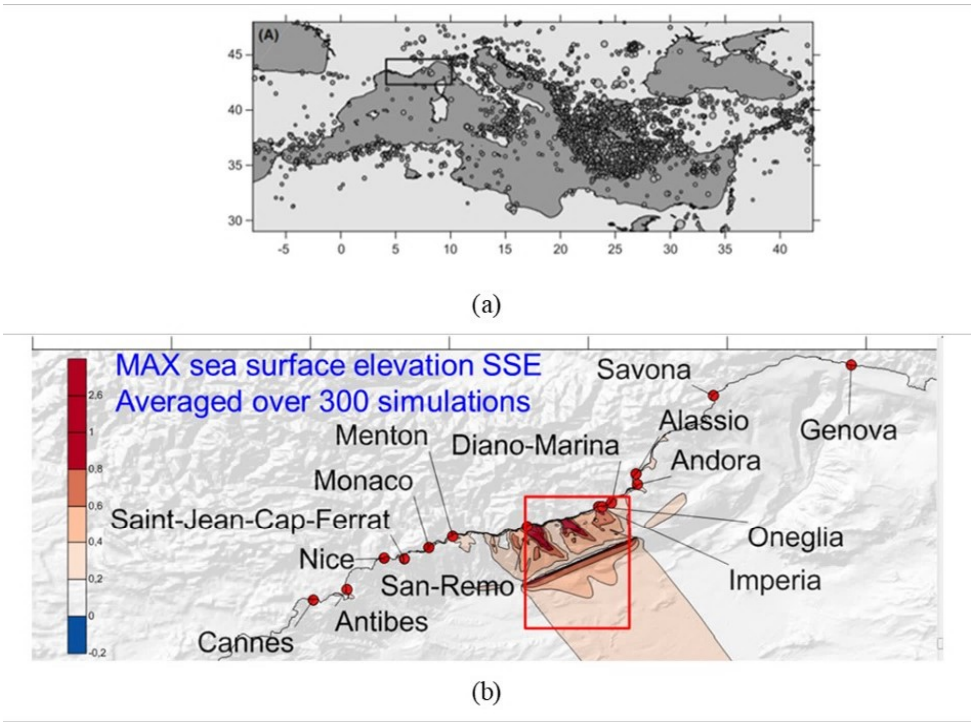

Figure 14: (a) Location of the test case for the development of the kriging-based procedure. (b) The coloured envelope corresponds to the map of maximum of sea surface elevation SSE averaged over 300 long-running simulations given the 1887 earthquake event (and the uncertainties on its characteristics).

These validated kriging metamodels were then used in place of the long running simulators within a Monte-Carlo setting (using 1,000 random draws) to evaluate the cumulative probability of SSE given the uncertainties on the worst-case scenario together with the metamodel errors. Figure 16 provides these probabilistic curves considering the different locations along the coast. These results can be useful to any Probabilistic Safety Analysis for NPP focused on tsunami hazard.

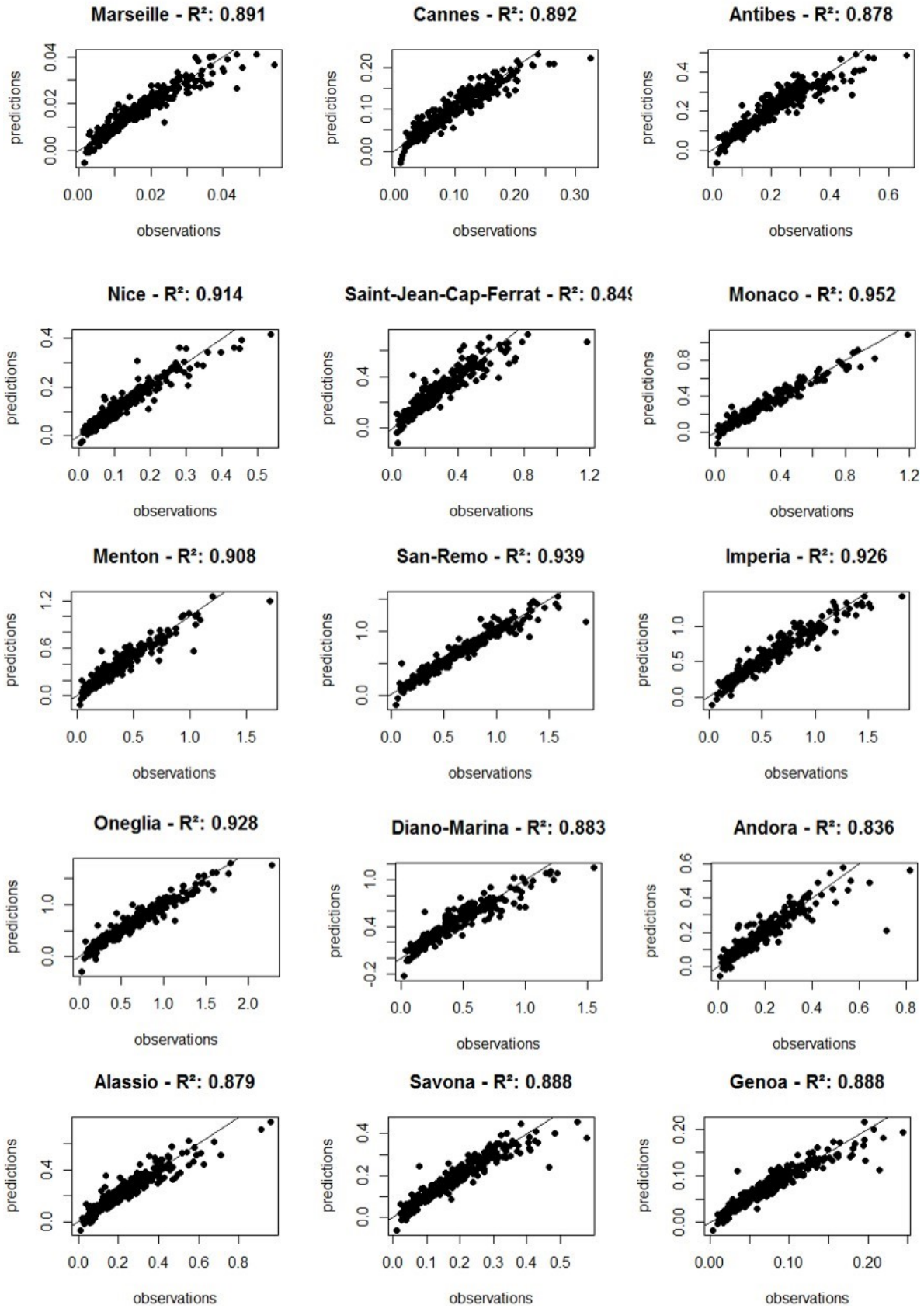

Figure 15: Comparison between observations (i.e. the results derived from the long running simulations) and the kriging-based predictions. The R^2 indicates whether the fit can be considered satisfactory (provided that the value exceeds at least 80%).

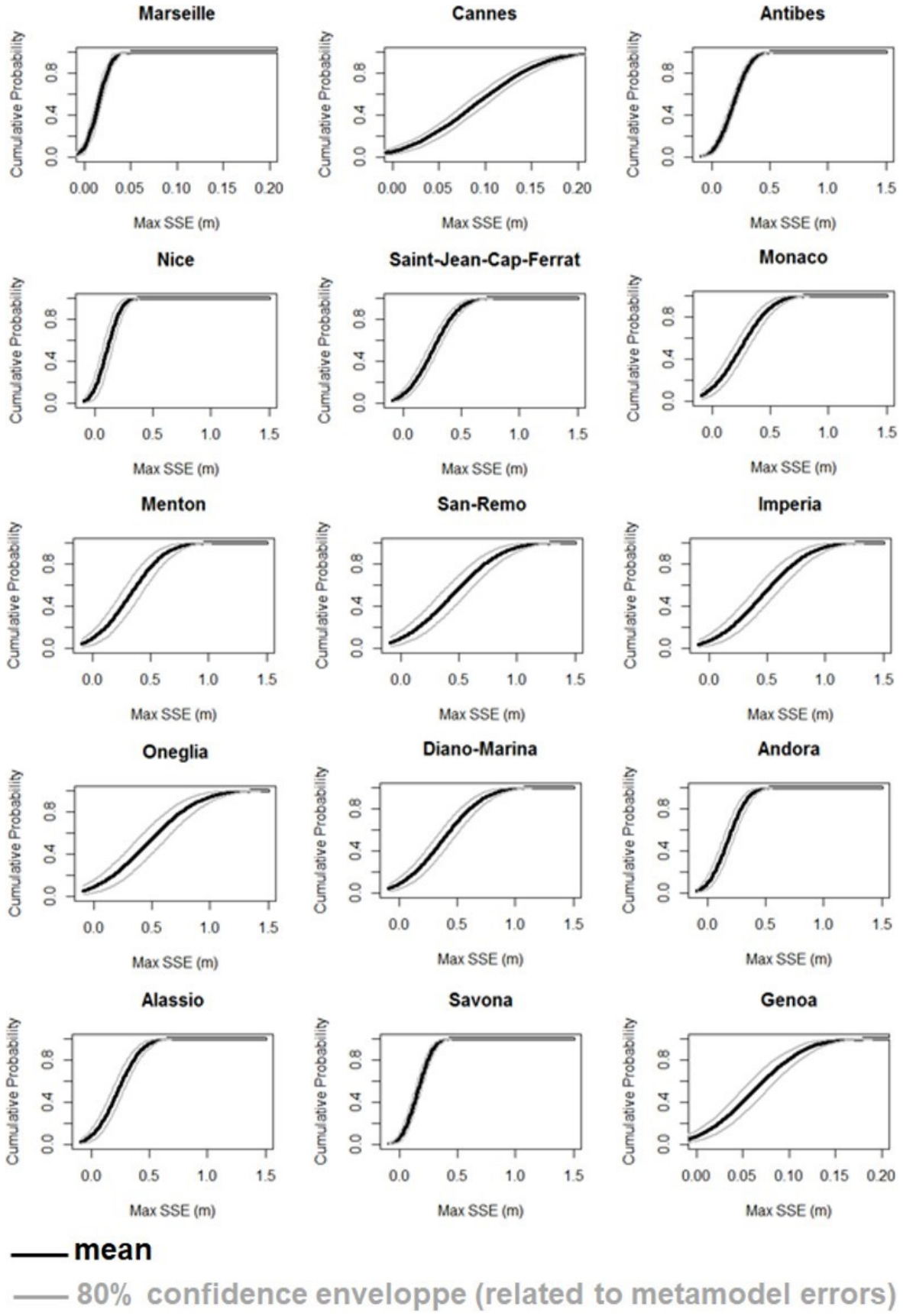

Figure 16: Cumulative Distribution Function for the maximum Sea Surface Elevation induced by the worst case scenario of the 1887 earthquake (plus the uncertainties on its characteristics) using the metamodels built along the coast.

4 Conclusion

In this report, different metamodeling strategies have been presented for probabilistic safety analyses of nuclear power plants submitted to tsunami and seismic hazards.

For seismic risks, the methodologies based on ANN and SVM show good performances in order to assess fragility curves when aleatory uncertainties have a predominant contribution in the variability of structural response. Once trained, the metamodels allows carrying out a large number of simulations for both parametric and non-parametric fragility analyses, at negligible computational cost.

Regarding the SVM-based methodology, it has been shown that a simple and universal preprocessing of the data (Box-Cox transformation of the input parameters) makes it possible to use a simple linear SVM to obtain a very precise classifier after only one hundred mechanical calculations. The advantage of a machine learning-based approach is that the input parameters of the earthquake ground motion model can be used additionally to the classical IM parameters to build the classifier and to improve its performance. For the class of structures considered, with only four classical seismic parameters (PGA, V, L, ω_0), it has been shown that the PGA-based or L-based fragility curves are very close to the reference curves obtained with a direct Monte Carlo-based approach.

The ANN based metamodel allows for introducing the residual or predictor uncertainty due to the reduction of the seismic signal to a set of scalar IMs. The feature selection algorithm allows for determining the most pertinent set of IMs in order to keep the residual uncertainty as low as possible. The ANN prediction uncertainty has been discussed thoroughly, the proposed approach allows for the identification of the aleatory and the epistemic uncertainty components in the ANN prediction uncertainties. Indeed, when computing fragility curves for seismic PSA of NPP, then it is important to properly distinguish aleatory and epistemic uncertainties since the latter determine the confidence bounds of failure probabilities and have a major impact on HCLPF. Also they should be propagated in failure and event trees to determine the confidence intervals of the final risk estimates in seismic PSA studies. Then, epistemic uncertainties can be reduced if more information or data is made available. The methodology has been applied to an industrial complex case study, i.e. Kashiwazaki-Kariwa nuclear power plant in Japan to evaluate the robustness of an electrical cabinet. The analyses conducted here show that the variability in the responses of the considered electrical cabinet is dominated by the seismic record-to-record randomness.

Whereas kriging does not seem relevant for seismic fragility curves assessments, it is successfully applied for uncertainty analysis of tsunami hazard assessments based on a worst case scenario (here by considering a historical case of the 19th century in the Mediterranean sea). In addition to overcoming the computaitonal burden related to uncertainty analysis with computer codes, this technique allows to incorporate the metamodel error in the analysis in order to highlight situations where the high confidnece in the metamodel-based prediction can be given, or conversely where cautious should be given.

5 References

[1] R. Sainct, C. Feau, J.-M. Martinez, J. Garnier, Efficient seismic fragility curve estimation by active learning on support vector machines, Submitted Structural Safety.doi:https://arxiv.org/abs/1810.01240.

[2] A. Armigliato, G. Pagnoni, F. Zaniboni, S. Tinti, Worst-case scenario approach to the tsunami hazard assessment for the coastal areas between augusta and siracusa, eastern sicily, italy, in: EGU General Assembly Conference Abstracts, Vol. 17, 2015.

[3] J. Rohmer, M. Rousseau, A. Lemoine, R. Pedreros, J. Lambert, A. Benki, Source characterisation by mixing long-running tsunami wave numerical simulations and historical observations within a metamodel-aided abc setting, Stoch. Environ. Res. Risk. Assess. 32(4) (2018) 967–984. doi:10.1007/s00477-017-1423-y.

[4] EPRI, Methodology for developing seismic fragilities, Tech. rep., Electric Power Research Institute EPRI, Palo Alto, CA, report TR-103959 (1994).

[5] R. Kennedy, C. Cornell, R. Campell, S. Kaplan, H. Perla, Probabilistic seismic safety study of an existing nuclear power plant, Nucl. Eng. Des. 59 (1980) 315–338. doi:10.1016/0029-5493(80)90203-4.

[6] C. Mai, K. Konakli, B. Sudret, Seismic fragility curves for structures using non-parametric representations, Front. Struct. Civ. Eng. 11 (2017) 169–186. doi:10.1007/s11709-017-0385-y.

[7] H. Y. Noh, D. Lallemant, A. S. Kiremidjian, Development of empirical and analytical fragility functions using kernel smoothing methods, Earthquake Eng. Struct. Dyn. 44 (2015) 1163–1180. doi:10.1002/eqe.2505.

[8] D. Lallemant, A. Kiremidjian, H. Burton, Statistical procedures for developing earthquake damage fragility curves, Earthquake Eng. Struct. Dyn. 44 (2015) 1373–1389. doi:10.1002/eqe.2522.

[9] M. Shinozuka, M. Q. Feng, J. Lee, T. Naganuma, Statistical analysis of fragility curves, J. Eng. Mech. 126 (2000) 1224–1231. doi:10.1061/(ASCE)0733-9399(2000)126:12(1224).

[10] I. Zentner, E. Borgonovo, Construction of variance-based metamodels for probabilistic seismic analysis and fragility assessment, Georisk 8 (2014) 202–216. doi:10.1080/17499518.2014.958173.

[11] V. U. Unnikrishnan, A. M. Prasad, B. N. Rao, Development of fragility curves using high-dimensional model representation, Earthquake Eng. Struct. Dyn. 42 (2013) 419–430. doi:10.1002/eqe.2214.

[12] N. Buratti, B. Ferracuti, M. Savoia, Response surface with random factors for seismic fragility of reinforced concrete frames, Struct. Saf. 32 (2010) 42–51. doi:10.1016/j.strusafe.2009.06.003.

[13] J. Seo, D. G. Linzell, Use of response surface metamodels to generate system level fragilities for existing curved steel bridges, Eng. Struct. 52 (2013) 642–653. doi:10.1016/j.engstruct.2013.03.023.

[14] J. Seo, L. Dueñas-Osorio, J. I. Craig, B. J. Goodno, Metamodel-based regional vulnerability estimate of irregular steel moment-frame structures subjected to earthquake events, Eng. Struct. 45 (2012) 585–597. doi:10.1016/j.engstruct.2012.07.003.

[15] S. K. Saha, V. Matsagar, S. Chakraborty, Uncertainty quantification and seismic fragility of base-isolated liquid storage tanks using response surface models, Probab. Eng. Mech. 43 (2016) 20–35. doi:10.1016/j.probengmech.2015.10.008.

[16] J. Park, P. Towashiraporn, Rapid seismic damage assessment of railway bridges using the response-surface statistical model, Struct. Saf. 47 (2014) 1–12. doi:10.1016/j.strusafe.2013.10.001.

[17] N. D. Lagaros, M. Fragiadakis, Fragility assessment of steel frames using neural networks, Earthquake Spectra 23 (2007) 735–752. doi:10.1193/1.2798241.

[18] N. D. Lagaros, Y. Tsompanakis, P. N. Psarropoulos, E. C. Georgopoulos, Computationally efficient seismic fragility analysis of geostructures, Comput. Struct. 87 (2009) 1195–1203. doi:10.1016/j.compstruc.2008.12.001.

[19] C. C. Mitropoulou, M. Papadrakakis, Developing fragility curves based on neural network IDA predictions, Eng. Struct. 33 (2011) 3409–3421. doi:10.1016/j.engstruct.2011.07.005.

[20] E. Ferrario, N. Pedroni, E. Zio, F. Lopez-Caballero, Application of metamodel-based techniques for the efficient seismic analysis of structural systems, in: Safety and Reliability of Complex Engineered Systems, ESREL, 2015, pp. 1193–1200.

[21] A. Calabresea, C. G. Lai, Fragility functions of blockwork wharves using artificial neural networks, Soil Dyn. Earthquake Eng. 52 (2013) 88–102. doi:10.1016/j.soildyn.2013.05.002.

[22] S. Mangalathu, J.-S. Jeon, R. DesRoches, Critical uncertainty parameters influencing seismic performance of bridges using lasso regression, Earthquake Eng. Struct. Dyn.doi:10.1002/eqe.2991.

[23] P. Gehl, D. D'Ayala, Development of bayesian networks for the multi-hazard fragility assessment of bridge systems, Struct. Saf. 60 (2016) 37–46. doi:10.1016/j.strusafe.2016.01.006.

[24] J. Ghosh, J. E. Padgett, L. Dueñas-Osorio, Surrogate modeling and failure surface visualization for ef ficient seismic vulnerability assessment of highway bridges, Probab. Eng. Mech. 34 (2013) 189–199. doi:10.1016/j.probengmech.2013.09.003.

[25] I. Gidaris, A. A. Taflanidis, G. P. Mavroeidis, Kriging metamodeling in seismic risk assessment based on stochastic ground motion models, Earthquake Eng. Struct. Dyn. 44 (2015) 2377–2399. doi:10.1002/eqe.2586.

[26] G. Jia, A. A.Taflanidis, Kriging metamodeling for approximation of high-dimensional wave and surge responses in real-time storm/hurricane risk assessment, Comput. Methods in Appl. Mech. Eng. 261–262 (2013) 24–38. doi:10.1016/j.cma.2013.03.012.

[27] C. V. Mai, M. D. Spiridonakos, E. N. Chatzi, B. Sudret, Surrogate modelling for stochastic dynamical systems by combining narx models and polynomial chaos expansions, International Journal for Uncertainty Quantification 6 (2016) 419–430. doi:10.1615/Int.J.UncertaintyQuantification.v6.i4.

[28] N. Ataei, J. E. Padgett, Fragility surrogate models for coastal bridges in hurricane prone zones, Eng. Struct. 103 (2015) 203–213. doi:10.1016/j.engstruct.2015.07.002.

[29] M. Hariri-Ardebili, V. Saouma, Probabilistic seismic demand model and optimal intensity measure for concrete dams, Structural Safety 59 (2016) 67–85. doi:https://doi.org/10.1016/j.strusafe.2015.12.001.
URL http://www.sciencedirect.com/science/article/pii/S0167473015000934

[30] R. Sanaz, Stochastic modeling and simulation of ground motions for performance-based earthquake engineering, Ph.D. thesis, University of California, Berkeley (2010).

[31] S. Rezaeian, A. Der Kiureghian, Simulation of synthetic ground motions for specified earthquake and site characteristics, Earthquake Engineering & Structural Dynamics 39 (10) (2010) 1155–1180. arXiv:https://onlinelibrary.wiley.com/doi/pdf/10.1002/eqe.997, doi:10.1002/eqe.997.
URL https://onlinelibrary.wiley.com/doi/abs/10.1002/eqe.997

[32] N. Ambraseys, P. Smit, R. Berardi, D. Rinaldis, F. Cotton, C. Berge, Dissemination of european strongmotion data, cD-ROM collection. European Commission, Directorate-General XII, Environmental and Climate Programme, ENV4-CT97-0397, Brussels, Belgium (2000).

[33] M. Kristan, A. Leonardis, D. Skočaj, Multivariate online kernel density estimation with gaussian kernels, Pattern Recognition 44 (10) (2011) 2630–2642. doi:https://doi.org/10.1016/j.patcog.2011.03.019.
URL http://www.sciencedirect.com/science/article/pii/S0031320311001233

[34] S. Tong, D. Koller, Support vector machine active learning with applications to text classification, J. Mach. Learn. Res. 2 (2002) 45–66. doi:10.1162/153244302760185243.
URL https://doi.org/10.1162/153244302760185243

[35] J. Kremer, K. Steenstrup Pedersen, C. Igel, Active learning with support vector machines, Wiley Int. Rev. Data Min. and Knowl. Disc. 4 (4) (2014) 313–326. doi:10.1002/widm.1132.
URL http://dx.doi.org/10.1002/widm.1132

[36] K. Trevlopoulos, C. Feau, I. Zentner, Parametric models averaging for optimized non-parametric fragility curve estimation based on intensity measure data clustering, Structural Safety 81 (2019) 101865. doi:https://doi.org/10.1016/j.strusafe.2019.05.002.
URL http://www.sciencedirect.com/science/article/pii/S0167473018302960

[37] C. A. Cornell, F. Jalayer, R. O. Hamburger, D. A. Foutch, Probabilistic basis for 2000 SAC federal emergency management agency steel moment frame guidelines, J. Struct. Eng. 128 (2002) 526–533. doi:10.1061/(ASCE)0733-9445(2002)128:4(526).

[38] M. Perrault, Evaluation de la vulnérabilité sismique de bâtiments à partir de mesures in situ, Ph.D. thesis, Université de Grenoble (2013).

[39] H. Xu, P. Gardoni, Probabilistic capacity and seismic demand models and fragility estimates for reinforced concrete buildings based on three-dimensional analyses, Eng. Struct. 112 (2016) 200–214. doi:10.1016/j.engstruct.2016.01.005.

[40] E. Ferrario, N. Pedroni, E. Zio, F. Lopez-Caballero, Bootstrapped artificial neural networks for the seismic analysis of structural systems, Struct. Saf. 67 (2017) 70–84. doi:10.1016/j.strusafe.2017.03.003.

[41] P. Towashiraporn, Building seismic fragilities using response surface metamodels, Ph.D. thesis, Georgia Institute of Technology (2004).

[42] C. M. Bishop, Neural Networks for Pattern Recognition, Oxford University Press, 1995.

[43] R. D. Reed, R. J. Marks, Neural Smithing, MIT Press, 1999.

[44] Z. Wang, N. Pedroni, I. Zentner, E. Zio, Seismic fragility analysis with artificial neural networks: Application to nuclear power plant equipment, Engineering Structures 162 (2018) 213 – 225. doi:https://doi.org/10.1016/j.engstruct.2018.02.024.
URL http://www.sciencedirect.com/science/article/pii/S0141029617326858

[45] N. Yoshida, S. Kobayashi, I. Suetomi, K. Miura, Equivalent linear method considering frequency dependent characteristics of stiffness and damping, Soil. Dyn. Earthq. Eng. 22 (2002) 205–222. doi:10.1016/S0267-7261(02)00011-8.

[46] I. Zentner, M. Gündel, N. Bonfils, Fragility analysis methods: Review of existing approaches and application, Nucl. Eng. Des.In press. doi:10.1016/j.nucengdes.2016.12.021.

[47] B. R. Ellingwood, K. Kinali, Quantifying and communicating uncertainty in seismic risk assessment, Struct. Saf. 31 (2009) 179–187. doi:10.1016/j.strusafe.2008.06.001.

[48] D. Rumelhart, G. Hinton, R. Williams, Learning Internal Representations by Error Propagation in Parallel Distributed Processing: Explorations in the Microstructure of Cognition, The MIT Press, 1986.

[49] N. Pedroni, E. Zio, G. Apostolakis, Comparison of bootstrapped artificial neural networks and quadratic response surfaces for the estimation of the functional failure probability of a thermal–hydraulic passive system, Reliab. Eng. Syst. Safe. 95 (2010) 386–395. doi:10.1016/j.ress.2009.11.009.

[50] E. Zio, A study of the bootstrap method for estimating the accuracy of artificial neural networks in predicting nuclear transient processes, IEEE T. Nucl. Sci. 53 (2006) 1460–1478. doi:10.1109/TNS.2006.871662.

[51] I. Rivals, L. Personnaz, Construction of confidence intervals for neural networks based on least squares estimation, Neural Networks 13 (2000) 463–484. doi:10.1016/S0893-6080(99)00080-5.

[52] G. Chryssoloiuris, M. Lee, A. Ramsey, Confidence interval prediction for neural network models, IEEE T. Neural Networ. 7 (1996) 229–232. doi:10.1109/72.478409.

[53] R. Dybowski, S. J. Roberts, Confidence intervals and prediction intervals for feed-forward neural networks, in: R. Dybowski, V. Gant (Eds.), Clinical Applications of Artificial Neural Networks, Cambridge University Press, 2001, pp. 298–326. doi:10.1016/S0933-3657(02)00081-7.

[54] Code_Aster, opensource Finite Element code, http://www.code-aster.org.

[55] MISS, a software in earthquake engineering and structural dynamics, http://www.mssmat.ecp.fr/miss.

[56] K. W. Campbell, Y. Bozorgnia, NGA ground motion model for the geometric mean horizontal component of PGA, PGV, PGD and 5% damped linear elastic response spectra for periods ranging from 0.01 to 10 s, Earthquake Spectra 24 (2008) 139–171. doi:10.1193/1.2857546.

[57] J. P. Stewart, S.-J. Chiou, J. D. Bray, R. W. Graves, P. G. Somerville, N. A. Abrahamson, Ground motion evaluation procedures for performance-based design, Tech. rep., Pacific Earthquake Engineering Research Center (2001).

[58] M. D. Biasio, S. Grange, F. Dufour, F. Allain, I. Petre-Lazar, Intensity measures for probabilistic assessment of non-structural components acceleration demand, Earthquake Eng. Struct. Dyn. 44 (2015) 2261–2280. doi:10.1002/eqe.2582.

[59] O. Ditlevesen, H. Madsen, Structural Reliability Methods, 2005.

[60] A. I. J. Forrester, A. K. A. Sobester, Engineering Design via Surrogate Modelling: A Practical Guide, John Wiley and Sons Ltd., Chichester, UK, 2008.

[61] O. Roustant, D. Ginsbourger, Y. Deville, Dicekriging, diceoptim: Two r packages for the analysis of computer experiments by kriging-based metamodelling and optimization, Journal of Statistical Software 51(1) (2012) 1–55. doi:10.18637/jss.v051.i01.

[62] T. Hastie, R. Tibshirani, J. Friedman, The Elements of Statistical Learning: Data Mining, Inference, and Prediction (2nd Edition), Springer-Verlag, New York, USA, 2009.

[63] S. T. Grilli, J. C. Harris, T. S. T. Bakhsh, T. L. Masterlark, C. Kyriakopoulos, J. T. Kirby, F. Shi, Numerical simulation of the 2011 tohoku tsunami based on a new transient fem co-seismic source: Comparison to far- and near-field observations, Pure Appl. Geophys. 170 (2013) 1333–1359. doi:10.1007/s00024-012-0528-y.

[64] Y. Okada, Surface deformation due to shear and tensile faults in a half-space, Bull. Seism. Soc. Am. 75 (1985) 1135–1154.

[65] J. Lambert, M. Terrier, Historical tsunami database for france and its overseas territories, Nat. Hazards Earth Syst. Sci. 11 (2011) 1037–1046.

[66] C. Larroque, O. Scotti, M. Ioualalen, Reappraisal of the 1887 ligurian earthquake (western mediterranean) from macroseismicity, active tectonics and tsunami modelling, Geophys. J. Int.doi:10.1111/j.1365-246X.2012.05498.x.

[67] M. Ioualalen, C. Larroque, O. Scotti, C. Daubord, Tsunami mapping related to local earthquakes on the french-italian riviera (western mediterranean), Pure Appl. Geophys. 171 (2014) 1423–1443. doi:10.1007/s00024-013-0699-1.

[68] F. Courboulex, A. Deschamps, M. Cattaneo, F. Costi, J. Deverchere, J. Virieux, P. Augliera, V. Lanza, D. Spallarossa, Source study and tectonic implications of the 1995 ventimiglia (border of italy and france) earthquake (ml = 4.7), Tectonophysics 290 (1998) 245–257. doi:10.1016/S0040-1951(98)00024-9.

[69] W. J. C. M. D. McKay, R. J. Beckman, A comparison of three methods for selecting values of input variables in the analysis of output from a computer code, Technometrics 21 (1979) 239–245.

[70] E. B. Consortium, EMODnet Digital Bathymetry (DTM), 2016. doi:10.12770/c7b53704-999d-4721-b1a3-04ec60c87238.